

# Effects of different discretisations of the Laplacian upon stochastic simulations of reaction-diffusion systems on both static and growing domains

Bartosz J. Bartmanski<sup>†</sup> and Ruth E. Baker<sup>†</sup>

<sup>†</sup>*Mathematical Institute, University of Oxford,  
Woodstock Road, Oxford, OX2 6GG, UK*

---

## Abstract

By discretising space into compartments and letting system dynamics be governed by the reaction-diffusion master equation, it is possible to derive and simulate a stochastic model of reaction and diffusion on an arbitrary domain. However, there are many implementation choices involved in this process, such as the choice of discretisation and method of derivation of the diffusive jump rates, and it is not clear *a priori* how these affect model predictions. To shed light on this issue, in this work we explore how a variety of discretisations and methods for derivation of the diffusive jump rates affect the outputs of stochastic simulations of reaction-diffusion models, in particular using Turing's model of pattern formation as a key example. We consider both static and uniformly growing domains and demonstrate that, while only minor differences are observed for simple reaction-diffusion systems, there can be vast differences in model predictions for systems that include complicated reaction kinetics, such as Turing's diffusion-driven instability model of pattern formation. Our work highlights that care must be taken in using the reaction-diffusion master equation framework to make predictions as to the dynamics of stochastic reaction-diffusion systems.

*Keywords:* stochastic simulation, diffusion, reaction, pattern formation.

*2010 MSC:* 35K05, 68U20, 65C35 92-08.

---

## 1. Introduction

Many biological processes hinge on the reaction and diffusion of constituent components and most of these are, in addition, subject to the inherent stochasticity of the natural world. Due to the non-linearity of interacting components, mathematical models provide a crucial means to interrogate how the combination of reaction and diffusion drive a given process. For example, mathematical models of reaction and diffusion have been used to model gene expression within a cell [4, 14, 15], cell invasion and colonisation processes [19, 31], and patterning of molecule distributions within a cell [11], to name but a few.

Models of reaction-diffusion systems can be roughly divided into macroscopic, mesoscopic and microscopic [10]. On the macroscale, partial differential equations (PDEs) are often used to model reaction-diffusion systems in terms of the evolution of species concentration in time and space. Such models can be analysed using a range of existing mathematical tools, however they do not take into account stochastic effects. At the other end of the spectrum we have microscopic descriptions such as stochastic differential equation (SDE) models, where each individual molecule is described in terms of its position and velocity, and molecules react when within a certain radius of each other [1]. Although such models provide a very detailed account of the reaction-diffusion process under consideration, they incur extremely high computational cost and are, as such, unfeasible for many real-world models [21, 29]. A mesoscopic description aims to strike a balance between the two, including descriptions of individual molecule dynamics without incurring prohibitive computational overheads. An example mesoscopic description is that of the reaction-diffusion master equation framework (RDME) [12, 13, 28]; in this model, the domain is discretised into compartments, molecules can react with other molecules in the same compartment, and diffusion is represented by jumps between neighbouring compartments. The RDME framework has been used to explore a range of biological phenomena, and it is this description of reaction and diffusion on which we focus in this work.

To model diffusion, the RDME framework requires computation of the rate per unit time of a molecule to jump from one compartment to a neighbouring one. Previous research in this direction includes the work by Engblom *et al.* [5], where the finite element method is used to calculate the diffusive jump rates, and that of Hellander and Petzold [10] who developed a description of diffusion for a more general compartment shapes.

In addition, Meinecke and Lötstedt explored the impact of different methods of diffusive jump rate derivation upon simulation of diffusive systems [16, 17, 18]. To mitigate issues with convergence of the RDME in the context of higher order reactions, Isaacson developed a convergent RDME that allows molecules to react even when they are not in the same compartment [13]. However, this approach does not consider how differences in the derivation of the diffusive jump rates affect model predictions.

### *1.1. Aims and outline*

Our aim in this work is to understand how the different methods of derivation of diffusive jump rates, and different domain discretisations, affect model predictions for reaction-diffusion systems on a two-dimensional domain, including those with bimolecular reactions and reaction kinetics capable of pattern formation. We will use Meinecke and Lötstedt’s [18] derivations of diffusive jump rates as a basis for our work. These derivations are based on three different numerical schemes: the finite difference method (FDM); the finite volume method (FVM); and the finite element method (FEM). In addition we include the fourth approach taken by Meinecke and Lötstedt that is based on first exit times (FETs) [18]. In Section 2 we outline the results of Meinecke and Lötstedt for a static domain [18], extend them to a uniformly growing domain, and present the stochastic simulation algorithm that we will use throughout this work. Our results are outlined in Section 3, including the effects of different diffusive jump rates on pattern formation in Section 3.1.4 and Section 3.1.5. A brief discussion of the results outlined in this paper can be found Section 4.

## **2. The reaction-diffusion master equation framework**

The chemical master equation (CME) framework describes the reaction of chemical species under the assumption that the molecules are well-mixed [24]. In general, the CME is intractable and, as a result, Gillespie [8] developed a stochastic simulation algorithm (SSA) to generate sample paths of the system under consideration. The RDME framework is an extension of the CME where the spatial domain is discretised into compartments, each of which is assumed well-mixed, and diffusion is modelled using a set of first-order reactions that describe the jumps of molecules between neighbouring compartments [24]. Again, the RDME is rarely tractable, and so stochastic simulation algorithms have been

developed to simulate reaction-diffusion systems modelled using the RDME framework [2, 9].

In this section, we outline the RDME framework, and the stochastic simulation algorithm that we will use throughout this work. For simplicity, we consider the evolution of a reaction-diffusion system in the square domain  $\Omega = [0, L] \times [0, L]$ , and partition  $\Omega$  using a Cartesian mesh into non-overlapping rectangular sub-domains  $C_i$ , called compartments, such that  $\Omega = \bigcup_{i=1}^I C_i$  (Figure 1) [18]. Each compartment is of size  $\kappa h \times h$ , where  $\kappa$  is the aspect ratio of a compartment, and the total number of compartments,  $I$ , can be expressed as  $I = n_x \times n_y$ , where  $n_x$  and  $n_y$  are the numbers of compartments in the  $x$ -direction and  $y$ -direction, respectively. We number the compartments starting at the bottom-left corner of the domain and then from left to right, so that, for site  $i$ , the adjacent compartments have indices  $i \pm 1$  in the  $x$ -direction and indices  $i \pm n_x$  in the  $y$ -direction.

We consider a reaction-diffusion system consisting of  $S$  species, where  $U_i^\varsigma(t)$  is the number of molecules of species  $\varsigma$  in compartment  $i$  at time  $t$ , for  $\varsigma = 1, \dots, S$  and  $i = 1, \dots, I$ . We define  $\mathbf{U}^\varsigma(t) = (U_1^\varsigma(t), \dots, U_I^\varsigma(t))$  to be the spatial vector of species  $\varsigma$  at time  $t$ ,  $\mathbf{U}(t) = (\mathbf{U}^1(t), \dots, \mathbf{U}^S(t))$  to be the state matrix of the system and  $\mathbb{P}(\mathbf{u}, t) = \mathbb{P}(\mathbf{U}(t) = \mathbf{u} | \mathbf{U}(0) = \mathbf{u}_0)$ . Changes to the state matrix occur through either reactions or diffusive jumps. We consider a system of  $r = 1, \dots, R$  chemical reactions such that reaction  $r$  has propensity function  $a_i^r$  in compartment  $i$  and is defined such that

$$a_i^r(\mathbf{u}(t))dt := \mathbb{P}(\text{reaction } r \text{ fires in compartment } i \text{ during } [t, t + dt) \text{ given the system is in state } \mathbf{u} \text{ at time } t), \quad (1)$$

where  $dt$  is an infinitesimal time interval. For more details of the specific forms of the propensity functions see [24]. Similarly, diffusive jumps have propensity function  $d_{i,j}^\varsigma$  where

$$d_{i,j}^\varsigma(\mathbf{u}(t))dt = \lambda_{i,j}^\varsigma u_i^\varsigma(t)dt, \quad (2)$$

is the probability that a molecule of species  $\varsigma$  jumps from compartment  $i$  to compartment  $j$  in the infinitesimal time interval  $[t, t + dt)$  given the system is in state  $\mathbf{u}$  at time  $t$ .

As such, the RDME can be written as

$$\begin{aligned} \frac{\partial}{\partial t} \mathbb{P}(\mathbf{u}, t) = & \sum_{i=1}^I \sum_{r=1}^R [a_i^r(\mathbf{u} - \boldsymbol{\nu}_{i,r}) \mathbb{P}(\mathbf{u} - \boldsymbol{\nu}_{i,r}, t) - a_i^r(\mathbf{u}) \mathbb{P}(\mathbf{u}, t)] \\ & + \sum_{i=1}^I \sum_{\substack{j=1 \\ j \neq i}}^I \sum_{\varsigma=1}^S [\lambda_{i,j}^{\varsigma}(u_i^{\varsigma}(t) + 1) \mathbb{P}(\mathbf{u} - \mathbf{e}_{i,j}^{\varsigma}, t) - \lambda_{i,j}^{\varsigma} u_i^{\varsigma}(t) \mathbb{P}(\mathbf{u}, t)], \end{aligned} \quad (3)$$

where  $\boldsymbol{\nu}_{i,r}$  is the stoichiometric matrix that describes the change in state upon firing of reaction  $r$  in compartment  $i$ , and  $\mathbf{e}_{i,j}^{\varsigma}$  is the stoichiometric matrix that describes the change in state upon a diffusive jump of a molecule of species  $\varsigma$  from compartment  $i$  to compartment  $j$  [12].

To generate sample paths for a reaction-diffusion system within the RDME framework described in Equation (3), we use an SSA called the next sub-volume method [2, 9]. Let  $t_i$  be the time until the next reaction within compartment  $i$  for  $i = 1, \dots, I$ , and let the total propensity for compartment  $i$  be

$$a_i^0(\mathbf{u}(t)) = \sum_{r=1}^R a_i^r(\mathbf{u}(t)) + \sum_{\substack{j=1 \\ j \neq i}}^I \sum_{\varsigma=1}^S d_{i,j}^{\varsigma}(\mathbf{u}(t)). \quad (4)$$

Then, given that  $T$  is the end time of a simulation, we can simulate sample paths consistent with the RDME in Equation (3) using the SSA given in Algorithm 1.

Although the RDME as outlined in Equation (3) and the accompanying text, together with the SSA of Algorithm 1, holds in full generality, for the rest of this work, we will assume for simplicity that all diffusion coefficients and reaction rates are spatially homogeneous.

### 2.1. Derivations of the diffusive jump rates on a static domain

We first consider a diffusion-only system with a single molecular species, U. As already outlined in Section 2, diffusion is modelled as a series of jumps between neighbouring compartments where the propensity function for a jump from compartment  $i$  to compartment  $j$  is  $d_{i,j}(\mathbf{u}(t)) = \lambda_{i,j} u_i(t)$ . Note that we have dropped the superscript  $\varsigma$  for clarity of notation since we are currently considering only a single species. In this work we will assume that  $\lambda_{i,j} = 0$ ,  $j = 1, \dots, I$ , unless  $j$  is one of the eight nearest neighbour compartments (indices  $i \pm 1$ ,  $i \pm n_x$  and  $i \pm (n_x \pm 1)$ ), as depicted in Figure 1. In this section we outline four methods for derivation of the  $\lambda_{i,j}$ .

---

**Algorithm 1** Next sub-volume method SSA

---

Set  $t = 0$ .

Initialise  $\mathbf{u}$ .

**for**  $i$  in  $\{1, 2, \dots, I\}$  **do**

    Initialise the time until the next reaction for compartment  $i$ :  $t_i \sim \exp(a_i^0(\mathbf{u}(t)))$ .

**end for**

**while**  $t < T$  **do**

    Find argmin of the set  $\{t_1, t_2, \dots, t_I\}$  and denote it  $m$ .

    Set  $t = t_m$ .

    Generate a random number  $r \sim U(0, 1)$ .

    Choose reaction / diffusion  $q$  to fire. Note that reaction  $k$  fires with probability  $a_i^k(\mathbf{u}(t))/a_i^0(\mathbf{u}(t))$  and diffusion of a molecule of species  $\varsigma$  from box  $i$  to box  $j$  occurs with probability  $d_{i,j}^\varsigma(\mathbf{u}(t))/a_i^0(\mathbf{u}(t))$ .

    Update molecule numbers:  $\mathbf{u} := \mathbf{u} + \boldsymbol{\nu}_q$ , where  $\boldsymbol{\nu}_q$  is the stoichiometric matrix of reaction / diffusion  $q$ .

    Let  $\Gamma$  be the set of indices of non-zero elements of  $\boldsymbol{\nu}_q$ .

**for**  $\gamma$  in  $\Gamma$  **do**

        Update  $a_\gamma^k(\mathbf{u}(t))$ ,  $d_{\gamma,j}^\varsigma(\mathbf{u}(t))$  and  $a_\gamma^0(\mathbf{u})$  accordingly.

        Generate a random number  $\Delta t \sim \exp(a_\gamma^0(\mathbf{u}))$ .

        Update the time until the next reaction:  $t_\gamma = t + \Delta t$ .

**end for**

**end while**

---

### 2.1.1. Diffusion of a single molecule

Consider a single molecule diffusing within the domain  $\Omega = [0, L] \times [0, L]$  with diffusion coefficient  $D$ . Then evolution of the position,  $\mathbf{x}(t) = (x(t), y(t))$ , of this molecule can be described using the following SDEs [6]:

$$x(t + dt) = x(t) + \sqrt{2D}dW_x, \quad (5)$$

$$y(t + dt) = y(t) + \sqrt{2D}dW_y, \quad (6)$$

where  $W_x$  and  $W_y$  are the usual Wiener processes, *i.e.*  $dW_x \sim N(0, dt)$  and  $dW_y \sim N(0, dt)$ . The associated Fokker-Planck equation (FPE) is

$$\frac{\partial p(\mathbf{x}, t)}{\partial t} = D\Delta p(\mathbf{x}, t) \quad \text{for } \mathbf{x} \in \Omega, \quad (7)$$

so that  $p(\mathbf{x}, t)d\mathbf{x}$  is the probability to find the molecule in the region  $[x, x + dx] \times [y, y + dy]$  at time  $t$ .

For simplicity, throughout this work we will use Neumann boundary conditions

$$(\mathbf{n} \cdot \nabla) p = 0 \quad \text{for } \mathbf{x} \in \partial\Omega, \quad (8)$$

and we take the initial distribution for the molecule position to be

$$p(\mathbf{x}, 0) = p_0(\mathbf{x}). \quad (9)$$

Using the Cartesian mesh shown in Figure 1, we discretise the Laplacian as follows:

$$D\Delta p(\mathbf{x}_i, t) \approx \sum_{j=1}^I \lambda_{i,j} \tilde{p}_j(t) - \sum_{j=1}^I \lambda_{j,i} \tilde{p}_i(t), \quad (10)$$

where  $\tilde{p}_i(t)$  is the approximate solution to Equation (7) at point  $\mathbf{x}_i$ , *i.e.* at the centre of compartment  $i$  at time  $t$ . The compartments are all of the same size,  $\kappa h \times h$ , with area  $A = \kappa h^2$  (Figure 1). Hence, exploiting translational symmetry and noting that the diffusion coefficient,  $D$ , is spatially homogeneous, we refer to the jump rates,  $\lambda_{i,j}$ , from now on as  $\lambda_n$  for  $n \in \{1, 2, \dots, 8\}$  (Figure 1), with

$$\lambda_0 = \sum_{n=1}^8 \lambda_n. \quad (11)$$

We now make a few remarks. First, note that this description allows for jumps between diagonally neighbouring compartments. Second, the indexing of the jump rates starts

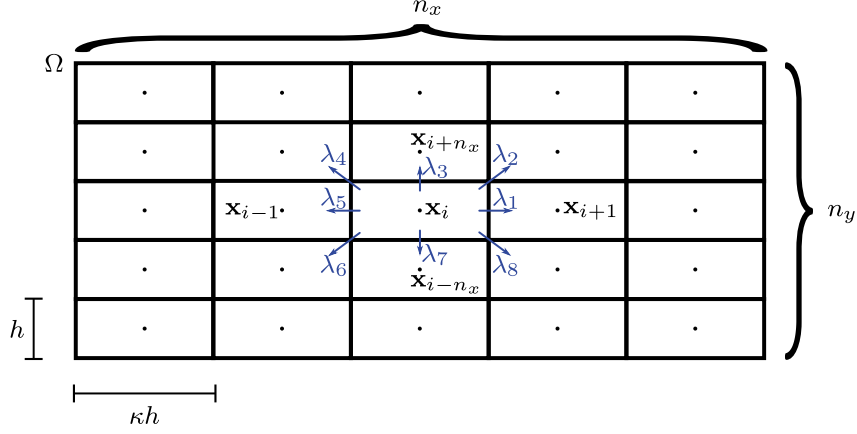


Figure 1: Schematic diagram of the discretisation of the two-dimensional domain  $\Omega$ , with the dimensions of the compartments and the indexing of the jump rates,  $\lambda_n$ , for  $n \in \{1, \dots, 8\}$  for a given compartment  $i$  shown.

at one for a jump to the right and continues in an anti-clockwise fashion, as shown in Figure 1. Third, due to the reflective symmetries of a Cartesian mesh, and since  $D$  is spatially homogeneous, we have the following identities

$$\lambda_1 = \lambda_5, \quad \lambda_3 = \lambda_7, \quad \lambda_2 = \lambda_4 = \lambda_6 = \lambda_8. \quad (12)$$

Finally, note that in what follows we present derivations of the jump rates for a two-dimensional domain. All the derivations naturally extend to three spatial dimensions, however care must be taken in deriving jump rates for those neighbouring voxels that do not share a face with the voxel under consideration, in particular those eight voxels that are “diagonal” neighbours.

### 2.1.2. The finite difference method

The first method we consider to derive the diffusive jump rates is the FDM. Meinecke and Lötstedt [18] chose a 9-point stencil which allows one to include a parameter  $\alpha$  to study the effects of diagonal jumps, while maintaining a discretisation of the Laplacian that is still second order accurate [26]. The standard 5-point stencil can be recovered by setting  $\alpha = 0$  and hence neglecting diagonal jumps. We have

$$\Delta p(\mathbf{x}_i, t) \approx \delta_x^2 \tilde{p}_i + \delta_y^2 \tilde{p}_i + \frac{1}{2} \alpha \kappa h^2 \delta_x^2 \delta_y^2 \tilde{p}_i, \quad (13)$$



144 where  $\alpha$  is a free parameter controlling the frequency of diagonal jumps, and the difference  
 145 operators are defined as follows:

$$\begin{aligned}\delta_x^2 \tilde{p}_i &= \frac{1}{\kappa^2 h^2} (\tilde{p}_{i+1} + \tilde{p}_{i-1} - 2\tilde{p}_i); \\ \delta_y^2 \tilde{p}_i &= \frac{1}{h^2} (\tilde{p}_{i+n_x} + \tilde{p}_{i-n_x} - 2\tilde{p}_i).\end{aligned}\tag{14}$$

146 As such, the right-hand side of Equation (7) can be approximated as

$$\begin{aligned}D\Delta p \approx & \frac{D - D\alpha\kappa}{\kappa^2 h^2} (\tilde{p}_{i+1} + \tilde{p}_{i-1}) + \frac{D\kappa - D\alpha}{\kappa h^2} (\tilde{p}_{i+n_x} + \tilde{p}_{i-n_x}) \\ & + \frac{D\alpha}{2\kappa h^2} (\tilde{p}_{i+n_x+1} + \tilde{p}_{i-n_x+1} + \tilde{p}_{i+n_x-1} + \tilde{p}_{i-n_x-1}) \\ & - 2D \frac{\kappa^2 - \alpha\kappa + 1}{\kappa^2 h^2} \tilde{p}_i.\end{aligned}\tag{15}$$

147 Comparing the general expression for the discretised Laplacian in Equation (10) with the  
 148 discretised Laplacian in Equation (15) we have

$$\lambda_1 = \frac{D - D\alpha\kappa}{\kappa^2 h^2},\tag{16}$$

$$\lambda_2 = \frac{D\alpha}{2\kappa h^2},\tag{17}$$

$$\lambda_3 = \frac{D\kappa - D\alpha}{\kappa h^2},\tag{18}$$

$$\lambda_0 = \frac{2D(\kappa^2 - \alpha\kappa + 1)}{\kappa^2 h^2}.\tag{19}$$

### 149 2.1.3. The finite volume method

150 We now consider derivation of the jump rates using the FVM. We start by averaging  
 151 the Laplacian at  $\mathbf{x}_i$  by integrating over compartment  $i$

$$D\Delta p(\mathbf{x}_i) \approx \frac{D}{A} \int_{C_i} \Delta p \, d\Omega,\tag{20}$$

152 where  $A$  is the area of the compartment  $i$ . Using the divergence theorem, we rewrite  
 153 Equation (20) as

$$D\Delta p(\mathbf{x}_i) \approx \frac{D}{A} \int_{\partial C_i} (\mathbf{n} \cdot \nabla) p \, ds,\tag{21}$$

154 where  $ds$  is a line element of the compartment boundary,  $\partial C_i$ , and  $\mathbf{n}$  is the normal vector  
 155 to the compartment boundary at the point  $\mathbf{x}$ .

156 Next, we split the integral in Equation (21) into integrals along segments of compart-  
 157 ment boundary  $\partial C_i$ , as shown in Figure 2,

$$D\Delta p(\mathbf{x}_i) \approx \frac{D}{A} \sum_{k=1}^4 \int_{\partial C_i^k} (\mathbf{n} \cdot \nabla) p \, ds,\tag{22}$$

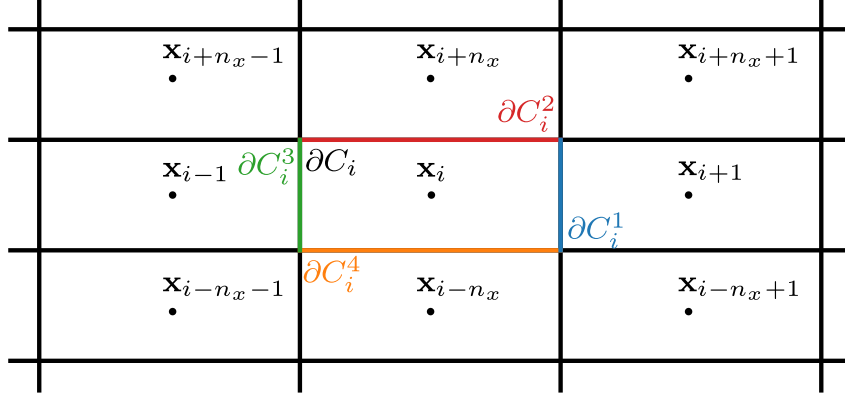


Figure 2: Schematic diagram of how compartment  $i$  boundary,  $\partial C_i$ , is split into four segments  $\partial C_i^k$  for  $k = 1, 2, 3, 4$ .

and we approximate the gradient of  $p$  across the different parts of the boundary of the compartment using a finite difference method:

$$\mathbf{n} \cdot \nabla p \Big|_{\partial C_i^1} \approx \frac{\tilde{p}_{i+1} - \tilde{p}_i}{\kappa h}, \quad (23)$$

$$\mathbf{n} \cdot \nabla p \Big|_{\partial C_i^2} \approx \frac{\tilde{p}_{i+n_x} - \tilde{p}_i}{h}, \quad (24)$$

$$\mathbf{n} \cdot \nabla p \Big|_{\partial C_i^3} \approx \frac{\tilde{p}_{i-1} - \tilde{p}_i}{\kappa h}, \quad (25)$$

$$\mathbf{n} \cdot \nabla p \Big|_{\partial C_i^4} \approx \frac{\tilde{p}_{i-n_x} - \tilde{p}_i}{h}. \quad (26)$$

Substituting Equations (23)–(26) into Equation (22) gives

$$\lambda_1 = \frac{D}{\kappa^2 h^2}, \quad (27)$$

$$\lambda_2 = 0, \quad (28)$$

$$\lambda_3 = \frac{D}{h^2}, \quad (29)$$

$$\lambda_0 = \frac{2D(\kappa^2 + 1)}{\kappa^2 h^2}. \quad (30)$$

#### 2.1.4. The finite element method

The last numerical method we will use to derive the jump coefficients is the FEM. We multiply Equation (7) by a test function  $w(\mathbf{x})$ , which is a function in Sobolev space [3] (*i.e.* is bounded and has bounded first partial derivatives), and integrate over the whole domain  $\Omega$ :

$$\begin{aligned} \int_{\Omega} \frac{\partial p}{\partial t} w \, dx \, dy &= D \int_{\Omega} w \Delta p \, dx \, dy \\ &= D \int_{\Omega} [\nabla \cdot (w \nabla p) - \nabla p \cdot \nabla w] \, dx \, dy. \end{aligned} \quad (31)$$

166 Now we use the divergence theorem to give

$$\int_{\Omega} \frac{\partial p}{\partial t} w \, dx \, dy = D \int_{\partial\Omega} \mathbf{n} \cdot [w \nabla p] \, ds - D \int_{\Omega} \nabla p \cdot \nabla w \, dx \, dy, \quad (32)$$

167 where  $ds$  is the line element of the domain boundary,  $\partial\Omega$ , and  $\mathbf{n}$  is the normal vector to  
 168 the domain boundary at the point  $\mathbf{x}$ . Due to the Neumann boundary conditions, the first  
 169 term in Equation (32) vanishes and we are left with

$$\int_{\Omega} \frac{\partial p}{\partial t} w \, dx \, dy = -D \int_{\Omega} \nabla p \cdot \nabla w \, dx \, dy. \quad (33)$$

170 We express the functions  $p$ ,  $\partial p / \partial t$  and  $w$  in terms of the basis functions  $\varphi_j$ ,

$$w(x, y) = \varphi_j(x, y), \quad (34)$$

$$p(x, y, t) \approx \sum_{i=1}^I \tilde{p}_i(t) \varphi_i(x, y), \quad (35)$$

$$\frac{\partial p}{\partial t}(x, y, t) \approx \sum_{i=1}^I \frac{d\tilde{p}_i}{dt}(t) \varphi_i(x, y), \quad (36)$$

171 where the  $\varphi_i$  are defined as

$$\varphi_i(x, y) = \begin{cases} \left(1 - \frac{x - x_i}{\kappa h}\right) \left(1 - \frac{y - y_i}{h}\right) & \text{for } \mathbf{x} \in [x_i, x_i + \kappa h] \times [y_i, y_i + h], \\ \left(1 + \frac{x - x_i}{\kappa h}\right) \left(1 - \frac{y - y_i}{h}\right) & \text{for } \mathbf{x} \in [x_i - \kappa h, x_i] \times [y_i, y_i + h], \\ \left(1 + \frac{x - x_i}{\kappa h}\right) \left(1 + \frac{y - y_i}{h}\right) & \text{for } \mathbf{x} \in [x_i - \kappa h, x_i] \times [y_i - h, y_i], \\ \left(1 - \frac{x - x_i}{\kappa h}\right) \left(1 + \frac{y - y_i}{h}\right) & \text{for } \mathbf{x} \in [x_i, x_i + \kappa h] \times [y_i - h, y_i], \\ 0 & \text{otherwise,} \end{cases} \quad (37)$$

172 for  $i \in \{1, \dots, I\}$ , and  $\varphi_j(\mathbf{x}) = 0$  for  $\mathbf{x} \notin \Omega$ . We choose linear basis functions for simplicity,  
 173 however, any form will suffice, as long as the following condition is met:

$$\varphi_j(x_i, y_i) = \begin{cases} 1 & \text{if } i = j; \\ 0 & \text{if } i \neq j. \end{cases} \quad (38)$$

174 Substituting Equations (34), (35) and (36) into Equation (33) gives, for each  $j$ ,

$$\sum_{i=1}^I \left( \int_{\Omega} \varphi_i \varphi_j \, dx \, dy \right) \frac{d\tilde{p}_i}{dt} = - \sum_{i=1}^I \left( \int_{\Omega} D \nabla \varphi_i \cdot \nabla \varphi_j \, dx \, dy \right) \tilde{p}_i, \quad (39)$$

Jump rates	FDM	FVM	FEM
$\lambda_1$	$\frac{D - D\alpha\kappa}{\kappa^2 h^2}$	$\frac{D}{\kappa^2 h^2}$	$\frac{D(2 - \kappa^2)}{3\kappa^2 h^2}$
$\lambda_2$	$\frac{D\alpha}{2\kappa h^2}$	0	$\frac{D(\kappa^2 + 1)}{6\kappa^2 h^2}$
$\lambda_3$	$\frac{D\kappa - D\alpha}{\kappa h^2}$	$\frac{D}{h^2}$	$\frac{D(2\kappa^2 - 1)}{3\kappa^2 h^2}$

Table 1: Comparison of jump rates from different derivations.

175 which can be expressed as a matrix equation

$$M \frac{d\tilde{\mathbf{p}}}{dt} = -N\tilde{\mathbf{p}}, \quad (40)$$

176 where

$$\tilde{\mathbf{p}} = (\tilde{p}_1, \tilde{p}_2, \dots, \tilde{p}_I), \quad (41)$$

$$M_{ij} = \int_{\Omega} \varphi_i \varphi_j \, dx \, dy, \quad (42)$$

$$N_{ij} = \int_{\Omega} D \nabla \varphi_i \cdot \nabla \varphi_j \, dx \, dy. \quad (43)$$

177 Evaluating the elements of the matrices  $M$  and  $N$ , and using the lumped mass matrix  
178 approach (see Section S1 of the Supplementary Information), we finally arrive at the  
179 following expressions for the jump coefficients:

$$\lambda_1 = \frac{D(2 - \kappa^2)}{3\kappa^2 h^2}; \quad (44)$$

$$\lambda_2 = \frac{D(\kappa^2 + 1)}{6\kappa^2 h^2}; \quad (45)$$

$$\lambda_3 = \frac{D(2\kappa^2 - 1)}{3\kappa^2 h^2}; \quad (46)$$

$$\lambda_0 = \frac{4D(\kappa^2 + 1)}{3\kappa^2 h^2}. \quad (47)$$

#### 180 2.1.5. The first exit time method

181 Meinecke and Löstedt proposed an additional method of calculating the jump rates [16,  
182 18]. This method involves considering the FET distribution from a domain  $\omega_i$  (centered

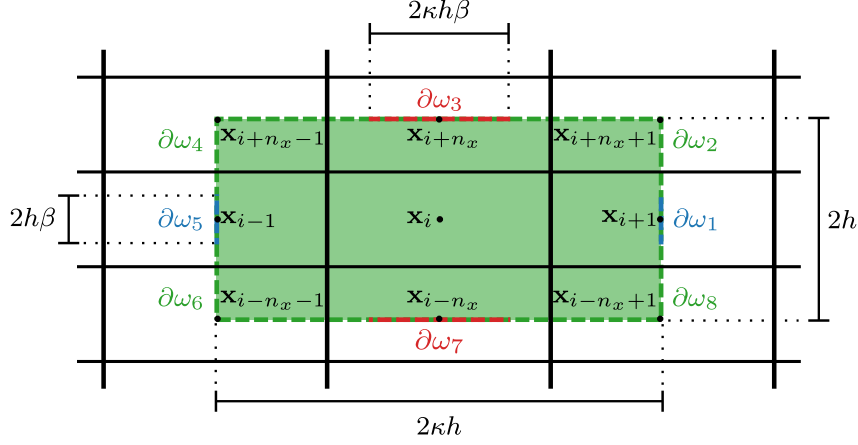


Figure 3: Diagram of the domain  $\omega_i$ , which has been shaded in green. The boundary of the domain  $\omega_i$ , indicated by the dashed line, is split into eight sections coloured as follows:  $\partial\omega_1$  is the rightmost blue;  $\partial\omega_2$  is the upper-right green;  $\partial\omega_3$  is the uppermost red;  $\partial\omega_4$  is the upper-left green;  $\partial\omega_5$  is the leftmost blue;  $\partial\omega_6$  is the lower-left green;  $\partial\omega_7$  is the lower red; and  $\partial\omega_8$  is the lower-right green.

on  $C_i$ ) of a single molecule undergoing Brownian motion that is placed initially at the centre of  $C_i$ . Note that to model diffusion in a RDME framework using FET-derived jump rates we approximate the probability distribution function (PDF) for the FET by an exponential distribution with the same mean. We follow the choice of domain  $\omega_i$  from [18], where  $\omega_i$  is defined by its boundary,  $\partial\omega_i$ , and taken to be a rectangle that intersects the centres of neighbouring compartments of compartment  $i$ , as shown in Figure 3, so that  $\omega_i$  completely contains the compartment  $i$ <sup>1</sup>.

We follow Meinecke and Löstedt [18] in choosing jump rates of the form

$$\lambda_n = \lambda_0 \theta_n, \quad (48)$$

where  $\theta_n$  is the probability that a molecule exits  $\omega_i$  into the  $n$ th neighbouring compartment (see Figure 1). We define a molecule to exit  $\omega_i$  into the  $n$ th neighbouring compartment if it exits through the segment of the domain boundary denoted by  $\partial\omega_i^n$  in Figure 3. There is flexibility in the choice of discretisation of the boundary  $\partial\omega_i$  into segments  $\partial\omega_i^n$ ,  $n = 1, \dots, 8$ , and we define the discretisation using parameter  $\beta$  as follows:

$$\begin{aligned} |\partial\omega_1| &= |\partial\omega_5| = 2\beta h; \\ |\partial\omega_3| &= |\partial\omega_7| = 2\beta \kappa h; \\ |\partial\omega_2| &= |\partial\omega_4| = |\partial\omega_6| = |\partial\omega_8| = (1 - \beta)(1 + \kappa)h. \end{aligned} \quad (49)$$

<sup>1</sup>The choice of  $\omega_i$  has been briefly discussed in [16] and so we do not explore it further here.

We will explore the effect of changing the parameter  $\beta$  on the jump rates in Section 2.1.6.

We proceed by considering two random variables associated with a molecule governed by Brownian motion exiting from the domain  $\omega_i$ :  $\tau$  and  $\eta$ . The random variable  $\tau$  denotes the FET out of  $\omega_i$ , whereas  $\eta$  denotes the exit segment. We use  $\tau$  to calculate  $\lambda_0$  by, as explained earlier, equating the mean of the PDF of  $\tau$  with the rate parameter of the exponential distribution used in Algorithm 1. The random variable  $\eta$ , on the other hand, is used to calculate  $\theta_n$ .

We calculate the PDF of  $\tau$  using the FPE (as outlined in Section 2.1) that describes the probability for the molecule to be at position  $\mathbf{x}$  at time  $t$ :

$$\frac{\partial p}{\partial t} = D\Delta p \quad \text{for } \mathbf{x} \in \omega_i, \quad (50)$$

where  $D$  is the diffusion coefficient. To calculate the PDF of the FET, we use Dirichlet (absorbing) boundary conditions

$$p(\mathbf{x}, t) = 0 \quad \text{for } \mathbf{x} \in \partial\omega_i, \quad (51)$$

and assume that initially the molecule is at the centre of  $\omega_i$  so that

$$p(\mathbf{x}, 0) = \delta(\mathbf{x} - \mathbf{x}_i). \quad (52)$$

Using  $p(\mathbf{x}, t)$  we calculate the survival probability,  $S(t)$ , which is the probability that a molecule remains in the domain  $\omega_i$  at least until time  $t$ , as [22]

$$S(t) = \mathbb{P}(\tau \geq t) = \int_{\omega_i} p(\mathbf{x}, t) d\omega, \quad (53)$$

where  $d\omega$  is a domain element of the domain  $\omega_i$ . Now, given  $S(t)$ , we derive the probability that a molecule exits  $\omega_i$  at time  $t$ , *i.e.* the PDF of the random variable  $\tau$ , denoted by  $\mathbb{P}(\tau = t)$ , as

$$\mathbb{P}(\tau = t) = -\frac{\partial S}{\partial t}. \quad (54)$$

Substituting Equation (53) into Equation (54) results in

$$\begin{aligned} \mathbb{P}(\tau = t) &= -\int_{\omega_i} \frac{\partial p}{\partial t} d\omega \\ &= -D \int_{\omega_i} \Delta p d\omega \\ &= -D \int_{\partial\omega_i} \mathbf{n} \cdot \nabla p ds, \end{aligned} \quad (55)$$

214 where  $ds$  is a line element of  $\partial\omega_i$ . Finally, we calculate the mean of the PDF for  $\tau$  as

$$E_\tau = \mathbb{E}[\tau] = \int_0^\infty t \mathbb{P}(\tau = t) dt = \int_0^\infty S(t) dt, \quad (56)$$

215 and set

$$\lambda_0 = \frac{1}{E_\tau}. \quad (57)$$

216 To calculate the PDF for  $\eta$  we use the law of total probability

$$\mathbb{P}(\eta = n) = \int_0^\infty \mathbb{P}(\eta = n | \tau = t) \mathbb{P}(\tau = t) dt. \quad (58)$$

217 Following [18], we have the probability of a molecule exiting through segment  $\partial\omega_i^n$  given  
218 that a molecule exits at time  $t$ , *i.e.* the probability  $\mathbb{P}(\eta = n | \tau = t)$ , as follows

$$\mathbb{P}(\eta = n | \tau = t) = \frac{\int_{\partial\omega_i^n} \mathbf{n} \cdot \nabla p ds}{\int_{\partial\omega_i} \mathbf{n} \cdot \nabla p ds}. \quad (59)$$

219 Substituting Equation (55) and Equation (59) into Equation (58) we have

$$\begin{aligned} \theta_n &= \mathbb{P}(\eta = n) \\ &= \int_0^\infty \frac{\int_{\partial\omega_i^n} \mathbf{n} \cdot \nabla p ds}{\int_{\partial\omega_i} \mathbf{n} \cdot \nabla p ds} \left( -D \int_{\partial\omega_i} \mathbf{n} \cdot \nabla p ds \right) dt \\ &= -D \int_0^\infty \int_{\partial\omega_i^n} \mathbf{n} \cdot \nabla p ds dt. \end{aligned} \quad (60)$$

220 Therefore, given solutions to Equation (48) and Equation (50), we can calculate the jump  
221 rates  $\lambda_n$  for  $n = 1, \dots, 8$ . To see the full expressions for the jump coefficients derived  
222 using the FET method see Section S2 of the Supplementary Information.

#### 223 2.1.6. Comparison of the diffusive jump rates

224 Figure 4 shows how the four methods of derivation compare to one another as the  
225 parameters  $\alpha$  and  $\beta$ , introduced during the derivations of the FDM and FET jump rates,  
226 respectively, are varied. Both  $\alpha$  and  $\beta$  control the frequency of diagonal jumps. For the  
227 FDM-derived jump rates, increasing the parameter  $\alpha$  increases  $\lambda_2$ , the rate of diagonal  
228 jumps. On the other hand, increasing  $\beta$  has the opposite effect on  $\lambda_2$  in the FET case.  
229 As the FEM- and the FVM-derived jump rates do not have any free parameters, they are  
230 constant in each of the plots.

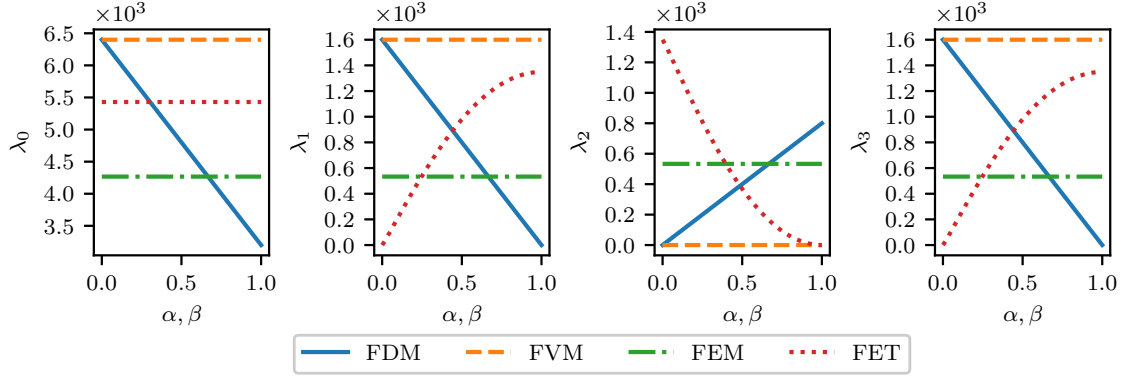


Figure 4: Plot of the jump rates as a function of the implementation parameters,  $\alpha$  and  $\beta$ , for  $h = 0.025 \mu m$ ,  $\kappa = 1.0$  and  $D = 1.0 \mu m^2 s^{-1}$  for the total jump rate,  $\lambda_0$ , as well as  $\lambda_1$ ,  $\lambda_2$  and  $\lambda_3$ . Since the derivations using the FEM and the FVM do not have any implementation parameters, the jump rates are constant for the given simulation parameters.

## 2.2. Derivation of the diffusive jump rates on a growing domain

The SDE description of a molecule undergoing Brownian motion on a two-dimensional growing domain  $\Omega_t = [0, L(t)] \times [0, L(t)]$  that we use in this work is

$$x(t + dt) = x(t) + v_x(x, y, t)dt + \sqrt{2D}dW_x, \quad (61)$$

$$y(t + dt) = y(t) + v_y(x, y, t)dt + \sqrt{2D}dW_y, \quad (62)$$

where the drift terms,  $v_x(x, y, t)$  and  $v_y(x, y, t)$ , describe the effects of domain growth.

The corresponding FPE is

$$\frac{\partial p}{\partial t} = D\nabla^2 p - \nabla \cdot (\mathbf{v}p) \quad \text{for } \mathbf{x} \in \Omega_t, \quad (63)$$

where  $\mathbf{v} = (v_x, v_y)$ , with Neumann boundary conditions

$$\nabla p|_{\partial\Omega_t} = 0, \quad (64)$$

and initial condition

$$p(\mathbf{x}, 0) = p_0(\mathbf{x}) \quad \text{for } \mathbf{x} \in \Omega_0, \quad (65)$$

where  $\mathbf{x} = (x, y)$ .

We will assume growth to be isotropic, *i.e.* for the domain to grow at the same rate in both  $x$ - and  $y$ -directions throughout this work, and so write

$$\mathbf{v}(\mathbf{x}, t) = (v_x, v_y) = \left( \frac{x\dot{L}(t)}{L(t)}, \frac{y\dot{L}(t)}{L(t)} \right). \quad (66)$$



As before, we wish to use different numerical methods to calculate how the probability that a molecule is in compartment  $i$  at time  $t$  changes over time, where compartment  $i$ , denoted  $C_i$ , is defined as

$$C_i = \left[ x_{i-\frac{1}{2}}(t), x_{i+\frac{1}{2}}(t) \right] \times \left[ y_{i-\frac{1}{2}}(t), y_{i+\frac{1}{2}}(t) \right]. \quad (67)$$

We calculate the probability for a molecule to be in  $C_i$  at time  $t$ ,  $\mathbb{P}(C_i, t)$ , by integrating the probability density function  $p(\mathbf{x}, t)$  over  $C_i$ :

$$\mathbb{P}(C_i, t) = \int_{x_{i-\frac{1}{2}}(t)}^{x_{i+\frac{1}{2}}(t)} \int_{y_{i-\frac{1}{2}}(t)}^{y_{i+\frac{1}{2}}(t)} p(\mathbf{x}, t) \, dx \, dy. \quad (68)$$

To proceed with the calculations we use a domain-fixing transformation, defining new coordinates as follows

$$(x, y, t) \rightarrow (\xi, \eta, \tau) = \left( \frac{x}{L(t)}, \frac{y}{L(t)}, t \right). \quad (69)$$

Under this transformation we have

$$\mathbb{P}(C_i, t) = \int_{\tilde{\xi}_{i-\frac{1}{2}}}^{\tilde{\xi}_{i+\frac{1}{2}}} \int_{\tilde{\eta}_{i-\frac{1}{2}}}^{\tilde{\eta}_{i+\frac{1}{2}}} p(\boldsymbol{\xi}, \tau) L^2(\tau) \, d\xi \, d\eta, \quad (70)$$

where  $\boldsymbol{\xi} = (\xi, \eta)$ , together with

$$\mathbf{v}(\boldsymbol{\xi}, \tau) = \boldsymbol{\xi} \frac{dL}{d\tau}. \quad (71)$$

Equation (63) becomes

$$\frac{\partial p}{\partial \tau} = \frac{D}{L^2(\tau)} \nabla_{\boldsymbol{\xi}}^2 p - \frac{2}{L(\tau)} \frac{dL}{d\tau} p \quad \text{for } \boldsymbol{\xi} \in \Omega_0, \quad (72)$$

where the advection term,  $\mathbf{v} \cdot \nabla p$ , from Equation (63) disappears due to the coordinate transformation described in Equation (69). Therefore the probability for a molecule to be in  $C_i$  at time  $t$  in the new coordinate system satisfies

$$\frac{\partial}{\partial \tau} \mathbb{P}(C_i, \tau) = \int_{\tilde{\xi}_{i-\frac{1}{2}}}^{\tilde{\xi}_{i+\frac{1}{2}}} \int_{\tilde{\eta}_{i-\frac{1}{2}}}^{\tilde{\eta}_{i+\frac{1}{2}}} \left\{ \frac{\partial p}{\partial \tau} L^2(\tau) + 2p(\boldsymbol{\xi}, \tau) L(\tau) \frac{dL}{d\tau} \right\} d\xi \, d\eta. \quad (73)$$

If we substitute Equation (72) into Equation (73) we have

$$\frac{\partial}{\partial \tau} \mathbb{P}(C_i, \tau) = \int_{\tilde{\xi}_{i-\frac{1}{2}}}^{\tilde{\xi}_{i+\frac{1}{2}}} \int_{\tilde{\eta}_{i-\frac{1}{2}}}^{\tilde{\eta}_{i+\frac{1}{2}}} \left\{ \left[ \frac{D}{L^2(\tau)} \nabla_{\boldsymbol{\xi}}^2 p - \frac{2}{L(\tau)} \frac{dL}{d\tau} p \right] L^2(\tau) + 2L(\tau) \frac{dL}{d\tau} p \right\} d\xi \, d\eta, \quad (74)$$

which leads to

$$\frac{\partial}{\partial \tau} \mathbb{P}(C_i, \tau) = \frac{D}{L^2(\tau)} \nabla_{\boldsymbol{\xi}}^2 \int_{\tilde{\xi}_{i-\frac{1}{2}}}^{\tilde{\xi}_{i+\frac{1}{2}}} \int_{\tilde{\eta}_{i-\frac{1}{2}}}^{\tilde{\eta}_{i+\frac{1}{2}}} p L^2(\tau) \, d\xi \, d\eta = \frac{D}{L^2(\tau)} \nabla_{\boldsymbol{\xi}}^2 \mathbb{P}(C_i, \tau), \quad (75)$$

where we note that the order of integration and differentiation can be exchanged due to Leibniz's integral rule. Therefore,  $\mathbb{P}(C_i, \tau)$  satisfies the diffusion equation with diffusion coefficient  $D/L^2(\tau)$ , and so we can simply use any method described in the Section 2.1 to discretise Equation (75) in order to derive the jump rates.

As an example, if we follow the steps in Section 2.1.3 to use the FVM to discretise Equation (75) we arrive at

$$\begin{aligned} \frac{\partial}{\partial t} \mathbb{P}(C_i, t) &= \frac{D}{\kappa^2 h^2(t)} (\mathbb{P}(C_{i+1}, t) + \mathbb{P}(C_{i-1}, t)) + \frac{D}{h^2(t)} (\mathbb{P}(C_{i+n_x}, t) + \mathbb{P}(C_{i-n_x}, t)) \\ &\quad - 2 \left( \frac{D}{\kappa^2 h^2(t)} + \frac{D}{h^2(t)} \right) \mathbb{P}(C_i, t), \end{aligned} \quad (76)$$

where  $h(t) = L(t)/n_y$ , similarly to the static domain case of  $h = L/n_y$ .

Therefore, by comparison of the coefficients in Equation (76), we see that the jump rates using the FVM are as follows

$$\lambda_1(t) = \frac{D}{\kappa^2 h^2(t)}, \quad (77)$$

$$\lambda_2(t) = 0, \quad (78)$$

$$\lambda_3(t) = \frac{D}{h^2(t)}, \quad (79)$$

with  $\lambda_0(t) = \sum_{i=1}^8 \lambda_i(t)$ .

The key advantage is that we can now simply use the diffusive jump rate derivations for the FDM, FVM and FEM on a static domain to write down the jump rates on the growing domain (see Table 2). Note that we no longer consider the FET approach to derive the diffusive jump rates. Simpson *et al.* [25] have previously shown that on a growing domain the survival probability does not approach zero in the limit  $t \rightarrow \infty$ . As a result, the FET distribution has infinite mean so we cannot use it to parameterise the exponential distribution as required in Equation (57).

### 3. Results

The SSA outlined in Algorithm 1 of Section 2 allows us to simulate a range of reaction-diffusion systems and test the impact of the different diffusive jump derivations on model predictions. We first explore a range of systems on a static domain, before moving to a growing domain.

Jump rates	FDM	FVM	FEM
$\lambda_1(t)$	$\frac{D - D\alpha\kappa}{\kappa^2 h^2(t)}$	$\frac{D}{\kappa^2 h^2(t)}$	$\frac{D(2 - \kappa^2)}{3\kappa^2 h^2(t)}$
$\lambda_2(t)$	$\frac{D\alpha}{2\kappa h^2(t)}$	0	$\frac{D(\kappa^2 + 1)}{6\kappa^2 h^2(t)}$
$\lambda_3(t)$	$\frac{D\kappa - D\alpha}{\kappa h^2(t)}$	$\frac{D}{h^2(t)}$	$\frac{D(2\kappa^2 - 1)}{3\kappa^2 h^2(t)}$

Table 2: Comparison of jump rates from different derivations on a growing domain.

### 3.1. Static domain

For simple systems, *e.g.* those that contain only zeroth and first order reactions, it is possible to compare results with analytic solutions of the corresponding macroscopic PDE models. The PDE represents the evolution of molecule concentration in time, so to compare with the results of a stochastic simulation, we use the following error measure:

$$e(t) = \sqrt{\sum_{i=1}^I A(t) \left| \frac{U_i(t)}{A(t)} - u(\mathbf{x}_i, t) \right|^2}, \quad (80)$$

where  $A(t)$  is the compartment area at time  $t$ , and  $u(\mathbf{x}_i, t)$  is the analytical solution of the corresponding macroscale PDE at  $\mathbf{x}_i$  at time  $t$ .

#### 3.1.1. Diffusion

We first investigate the effects of varying the compartment aspect ratio,  $\kappa$ . The macroscale PDE that describes the evolution of molecule concentration is

$$\frac{\partial u(\mathbf{x}, t)}{\partial t} = D\Delta u(\mathbf{x}, t) \quad \text{for } \mathbf{x} \in \Omega, \quad (81)$$

with Neumann boundary conditions

$$(\mathbf{n} \cdot \nabla) p = 0 \quad \text{for } \mathbf{x} \in \partial\Omega, \quad (82)$$

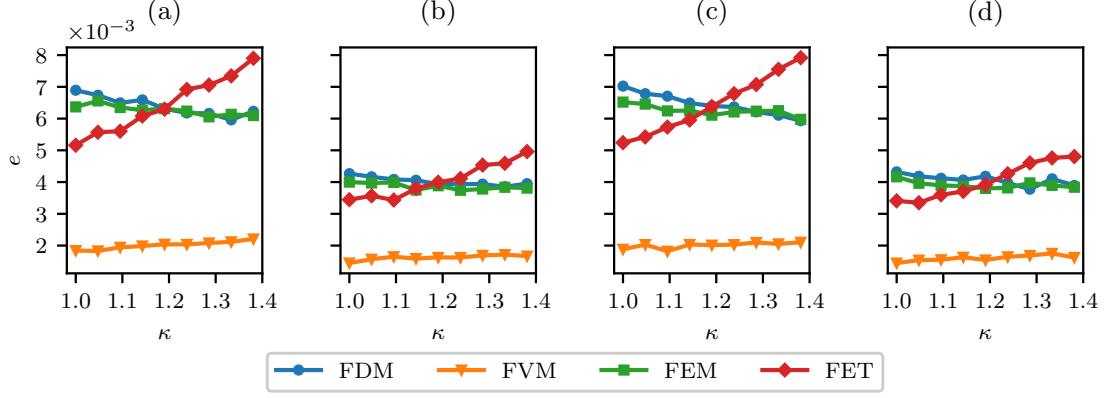


Figure 5: Plot of the error, as defined in Equation (81), as a function of  $\kappa$ , the compartment aspect ratio, for simulations with (a) diffusion only, (b) diffusion and production, (c) diffusion and decay and (d) diffusion, decay and production. The domain  $\Omega = [0, 20] \times [0, 20] \mu m^{-2}$  is discretised into  $21 \times 21\kappa$  compartments and  $5 \times 10^6$  molecules are placed initially in the central compartment. Parameters are:  $D = 1 \mu m^2 s^{-1}$ ,  $\alpha = 0.7$ ,  $\beta = 0.5$ ,  $T = 5 s$  and  $k_1 = 100 \mu m^{-2} s^{-1}$ ,  $k_{-1} = 0.1 s^{-1}$  for the systems involving production and decay, respectively.

where  $\mathbf{n}$  is the normal vector to the domain boundary  $\partial\Omega$ . We choose the initial condition to be

$$u(\mathbf{x}, 0) = \begin{cases} 5 \times 10^6 / A & \text{for } 0 < x < \kappa h, \ 0 < y < h, \\ 0 & \text{otherwise.} \end{cases} \quad (83)$$

We use the analytic solution of this PDE to calculate the error,  $e(t)$ , using Equation (81).

Separation of variables gives

$$\begin{aligned} u(\mathbf{x}, t) = & \frac{u_0 \kappa h^2}{L^2} \\ & + \sum_{n=1}^{\infty} \frac{2u_0 h}{n\pi L} \sin\left(\frac{n\pi \kappa h}{L}\right) \cos\left(\frac{n\pi x}{L}\right) \exp\left(-Dt \left(\frac{n\pi}{L}\right)^2\right) \\ & + \sum_{m=1}^{\infty} \frac{2u_0 \kappa h}{m\pi L} \sin\left(\frac{m\pi h}{L}\right) \cos\left(\frac{m\pi y}{L}\right) \exp\left(-Dt \left(\frac{m\pi}{L}\right)^2\right) \\ & + \sum_{n=1}^{\infty} \sum_{m=1}^{\infty} \frac{4u_0}{nm\pi^2 L^2} \sin\left(\frac{n\pi \kappa h}{L}\right) \sin\left(\frac{m\pi h}{L}\right) \cos\left(\frac{m\pi x}{L}\right) \cos\left(\frac{n\pi y}{L}\right) \\ & \times \exp\left(-Dt \left(\frac{(m^2 + n^2)\pi^2}{L^2}\right)\right). \end{aligned} \quad (84)$$

Figure 5(a) shows that the error is relatively unaffected by variation in the compartment aspect ratio,  $\kappa$ . For the values of  $\alpha$  and  $\beta$  used, the FVM-derived jump rates give rise to the smallest error, while the other methods (FDM, FEM and FET) lead to errors that are very similar to each other. Note that for  $\alpha = 0$  the diffusive jump rates for the FDM and the FVM are identical, indicating that increasing  $\alpha$  increases the error.

### 3.1.2. Zeroth and first order reactions

We now consider reaction-diffusion systems involving the decay of molecules, given by the chemical equation



and the production of molecules, given by the chemical equation



alongside diffusion. The corresponding propensity functions take the form

$$a_i^{\text{decay}}(\mathbf{u}(t)) = k_{-1}u_i(t), \quad (87)$$

$$a_i^{\text{prod}}(\mathbf{u}(t)) = k_1A(t), \quad (88)$$

for the decay reaction and the production reaction in compartment  $i$ , respectively. As before,  $A(t)$  is the area of a compartment at time  $t$ , and  $u_i(t)$  is the number of molecules in compartment  $i$  at time  $t$ . We consider production-only, decay-only and production-and-decay systems, and the macroscale PDEs that describe the evolution of molecule concentration are, respectively,

$$\frac{\partial u(\mathbf{x}, t)}{\partial t} = D\Delta u(\mathbf{x}, t) + k_1, \quad (89)$$

$$\frac{\partial u(\mathbf{x}, t)}{\partial t} = D\Delta u(\mathbf{x}, t) - k_{-1}u, \quad (90)$$

$$\frac{\partial u(\mathbf{x}, t)}{\partial t} = D\Delta u(\mathbf{x}, t) + k_1 - k_{-1}u. \quad (91)$$

Again, we use Neumann boundary conditions

$$(\mathbf{n} \cdot \nabla) p = 0 \quad \text{for } \mathbf{x} \in \partial\Omega, \quad (92)$$

where  $\mathbf{n}$  is the normal vector to the domain boundary  $\partial\Omega$ , and initially  $5 \times 10^6$  molecules are placed in the lower-left compartment of the domain. Given the above PDEs, we can use the previously calculated analytic solution in Equation (85), which we denote as  $\tilde{u}(\mathbf{x}, t)$ , to calculate the analytical solutions to Equations (90)–(92). The analytical solution to Equation (90) is

$$u(\mathbf{x}, t) = \tilde{u}(\mathbf{x}, t) + k_1t, \quad (93)$$

the solution to Equation (91) is

$$u(\mathbf{x}, t) = \tilde{u}(\mathbf{x}, t)e^{-k_{-1}t}, \quad (94)$$

and, finally, the analytical solution to Equation (92) is

$$u(\mathbf{x}, t) = \tilde{u}(\mathbf{x}, t)e^{-k_{-1}t} + \frac{k_1}{k_{-1}} (1 - e^{-k_{-1}t}). \quad (95)$$

When evaluating any of these analytical solutions numerically, we truncate the sum to the first million terms.

Figures 5(b)–(d) show how the error,  $e(t)$ , varies with  $\kappa$ . Again, the FVM out-performs the other three methods (FDM, FEM and FET) for the chosen values of  $\alpha$  and  $\beta$ . In addition, for systems involving decay (a first order reaction) the error increases as the aspect ratio of the compartments,  $\kappa$ , increases.

### 3.1.3. Second-order reactions

To investigate the effects of different derivations of the jump rates in systems involving second-order reactions, we now consider a system composed of two species, U and V, which undergo diffusion (with rates  $D_u$  and  $D_v$ , respectively) and the following reactions



*i.e.* U is consumed upon contact with V at rate  $k_1$ , and U is produced at rate  $k_2$ . The corresponding propensity functions take the form

$$a_i^1(\mathbf{u}(t)) = \frac{k_1}{A(t)} u_i(t) v_i(t), \quad (97)$$

$$a_i^2(\mathbf{u}(t)) = k_2 A(t). \quad (98)$$

We cannot write down equivalent closed-form macroscale PDEs for the evolution of the concentrations of U and V over time because the system contains second order reactions. As such, we investigate how the stationary distribution, estimated from stochastic simulations, is affected by the choice of compartment size, for the four different methods of deriving the diffusive jump rates. In Figure 6(a) we see that as the number of compartments increases the stationary distribution shifts to the right, towards higher molecule numbers. This is because the effective rate of bimolecular reactions decreases as the number of compartments increases [13]. Figures 6(b)–(d) show how the stationary distribution changes with the method of derivation of the diffusive jump rates. All methods give slightly different results; in particular, using  $\beta = 0.1$  or  $\beta = 0.9$  in the FET method results in stationary distributions that are shifted noticeably to the left (Figure 6(d)). We also note that the derivation parameters  $\alpha$  and  $\beta$  do not have a significant effect on

the stationary distributions presented in Figures 6(b) and (d). For  $\alpha$ , and the range over which  $\beta$  is varied, these results are consistent with other example cases investigated in this work.

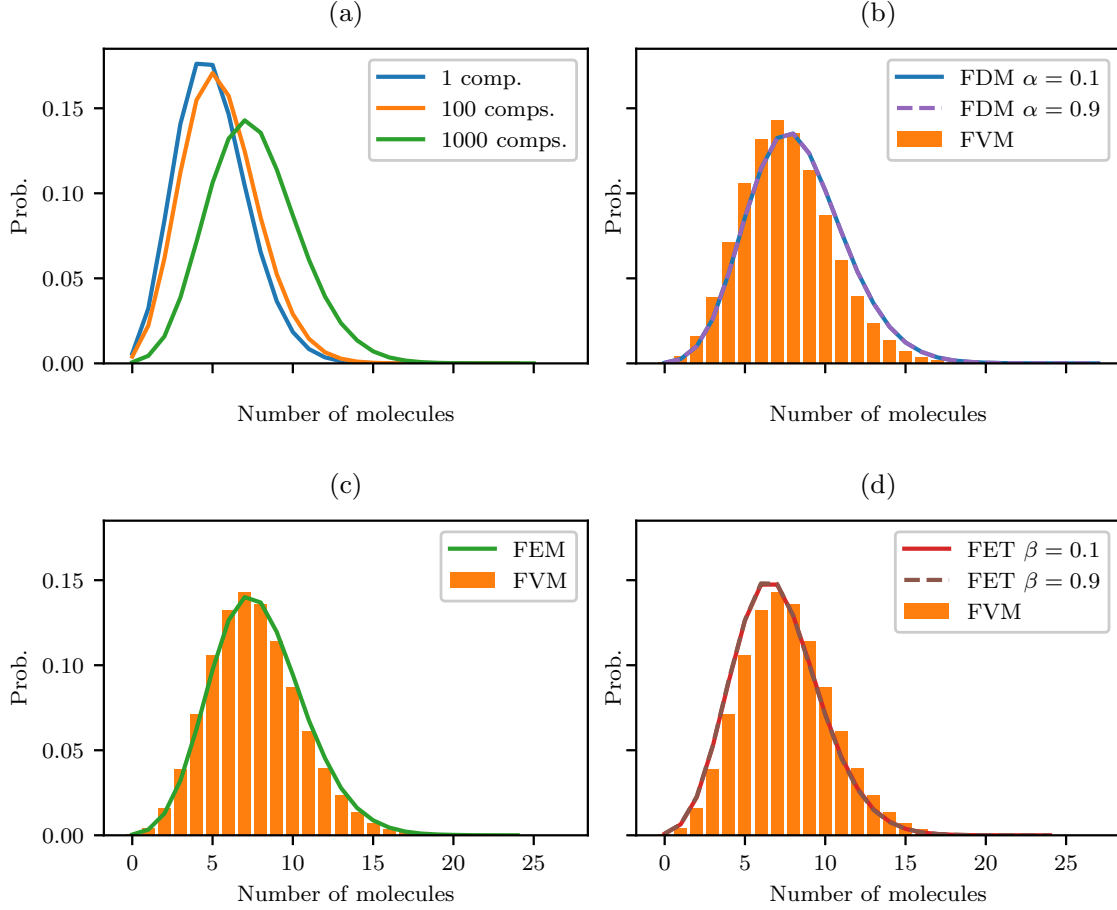
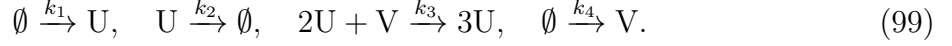


Figure 6: Stationary distributions as calculated from simulations run until  $T = 1 \times 10^6 s$ , on the domain  $\Omega = [0, 1] \times [0, 1] \mu m^{-2}$ , with the following reaction rates:  $k_1 = 0.2 \mu m^2 s^{-1}$  and  $k_2 = 1.0 \mu m^{-2} s^{-1}$ . We initialised the simulations with five molecules of U and one molecule of V distributed at random across the compartments. (a) Comparison of the stationary distributions as the compartment number is varied, where we used FVM-derived jump rates. (b), (c), (d) Comparison of the stationary distributions for different methods of derivation of the diffusive jump rates. The domain has been discretised into  $1000 \times 1000$  compartments.

### 3.1.4. Schnakenberg kinetics

Next, we investigate the effects of different derivations of diffusive jump rates on Turing's reaction-diffusion model of pattern formation [27]. We focus on Schnakenberg kinetics [7, 23] as they are simple to simulate. The system is composed of two species, U and V, which undergo diffusion (with rates  $D_u$  and  $D_v$ , respectively) and the following reactions



The corresponding propensity functions take the form

$$a_i^1(\mathbf{u}(t), \mathbf{v}(t)) = k_1 A(t), \quad (100)$$

$$a_i^2(\mathbf{u}(t), \mathbf{v}(t)) = k_2 u_i(t), \quad (101)$$

$$a_i^3(\mathbf{u}(t), \mathbf{v}(t)) = \frac{k_3}{A(t)^2} u_i(t)(u_i(t) - 1)v_i(t), \quad (102)$$

$$a_i^4(\mathbf{u}(t), \mathbf{v}(t)) = k_4 A(t). \quad (103)$$

We quantify the patterns formed using the discrete Fourier cosine transform. Let  $f(x, y) : \mathbb{R}^2 \rightarrow \mathbb{R}$ , then the discrete Fourier cosine transform is defined as

$$\hat{f}(k_x, k_y, t) = \Delta_x \Delta_y \sum_{i=1}^{n_x} \sum_{j=1}^{n_y} \cos(k_x \Delta_x (i - 1)) \cos(k_y \Delta_y (j - 1)) f(x, y, t), \quad (104)$$

where  $\Delta_x$  is the spacing between points  $\mathbf{x}_i$  and  $\mathbf{x}_{i+1}$  and  $\Delta_y$  is the spacing between points  $\mathbf{x}_i$  and  $\mathbf{x}_{i+n_x}$  (here,  $\Delta_x = \kappa h$  and  $\Delta_y = h$ ). The wavenumbers,  $k_x$  and  $k_y$ , give the spatial frequency of a pattern, with wavemodes  $m_x$  and  $m_y$  such that  $k_x = m_x \pi / L$  and  $k_y = m_y \pi / L$ , where  $L$  is the side length of the square domain  $\Omega$  [33]. To showcase results, we plot the power spectrum, defined as

$$P_s(t) = \left| \hat{f}(k_x, k_y, t) \right|^2, \quad (105)$$

where  $\hat{f}(\cdot, \cdot)$  is the discrete Fourier cosine transform defined in Equation (105).

We can predict which patterns are possible in equivalent PDE models of pattern formation using linear stability analysis (LSA) [20] (see Section S3 of the Supplementary Information for more details). In addition, Woolley *et al.* [32] developed a method using a weak noise expansion (WNE) of the RDME [28] to determine the wavemodes that can evolve in stochastic simulations (see Section S4 of the Supplementary Information for more details). The advantage of the WNE approach over LSA in determining whether



a particular wavemode is possible for a given parameter set is that the WNE approach takes into account the details of the diffusive jump rates. We compare the simulation results to the predictions of the WNE and LSA to see whether the patterns formed fall within the ranges of wavemodes predicted by those methods.

All the simulations are run until  $T = 1800\text{ s}$  on the domain  $\Omega = [0, 1] \times [0, 1] \mu\text{m}^{-2}$ , which is discretised into  $40 \times 40\kappa$  compartments, for either  $\kappa = 1.0$  or  $\kappa = 1.4$ , as stated within the figures. We use the following reaction rates:  $D_u = 1 \times 10^{-5} \mu\text{m}^2\text{s}^{-1}$ ,  $D_v = 1 \times 10^{-3} \mu\text{m}^2\text{s}^{-1}$ ,  $k_1 = 1\text{ s}^{-1}$ ,  $k_2 = 0.02\text{ s}^{-1}$ ,  $k_3 = 1 \times 10^{-6}\text{ s}^{-1}$  and  $k_4 = 3\text{ s}^{-1}$ . We initialise the system at the spatially uniform steady state, placing 200 molecules of species U and 75 molecules of species V in each compartment, and note that by  $T = 1800\text{ s}$  the patterns appear to have stopped evolving in time.

373 *The finite difference method.* The left-most column of Figure 7 shows examples of pat-  
 374 terns formed with FDM-derived diffusive jump rates, while the second-from-left column of  
 375 Figure 7 shows corresponding power spectra averaged over 100 simulations. There is good  
 376 agreement with the possible wavemodes predicted using the WNE (right-most column of  
 377 Figure 7) and LSA (second-from-right column of Figure 7). Our results indicate that  
 378 varying the parameter  $\alpha$ , which controls the rate of diagonal jumping, has no discernible  
 379 effect on pattern formation, except when  $\alpha = 1.0$  (only diagonal jumps are possible) where  
 380 checkerboard patterns arise.

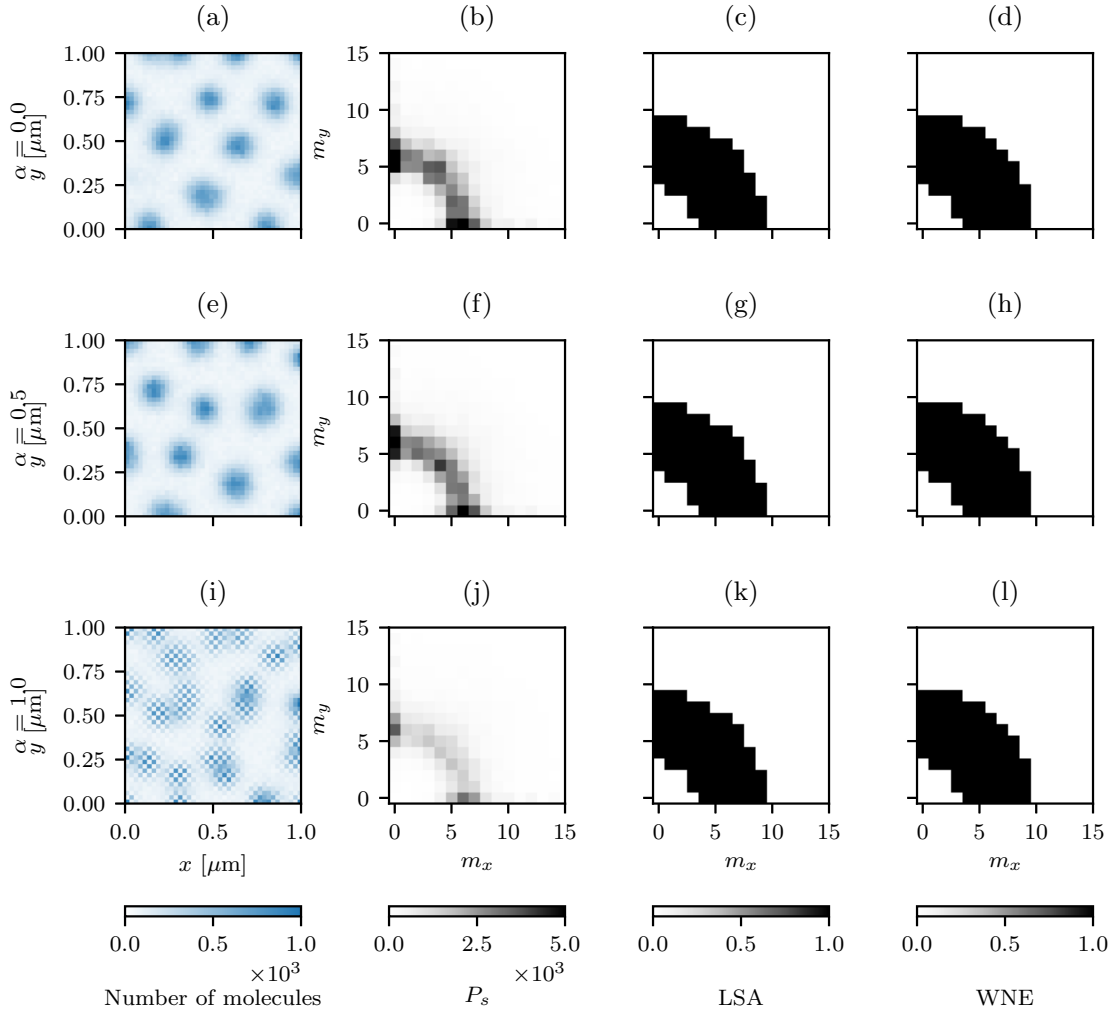


Figure 7: Results from simulations with FDM-derived diffusive jump rates with  $\kappa = 1.0$ . (a), (e), (i) An example pattern of species U. (b), (f), (j) Averaged power spectrum over 100 simulations. (c), (g), (k) Wavemodes predicted using LSA. (d), (h), (l) Wavemodes predicted using the WNE. In the plots that show predicted wavemodes using LSA and the WNE, the points at which a wavemode is predicted have a value of 1, and 0 otherwise.

381 *The finite volume method.* For the case of FVM-derived diffusive jump rates, the simula-  
 382 tions produced very similar results to the FEM-derived diffusive jump rates. The averaged  
 383 power spectrum, as well as the predicted wavemodes using LSA and the WNE, are very  
 384 similar for the FVM and FEM cases, as can be seen in Figure 8.

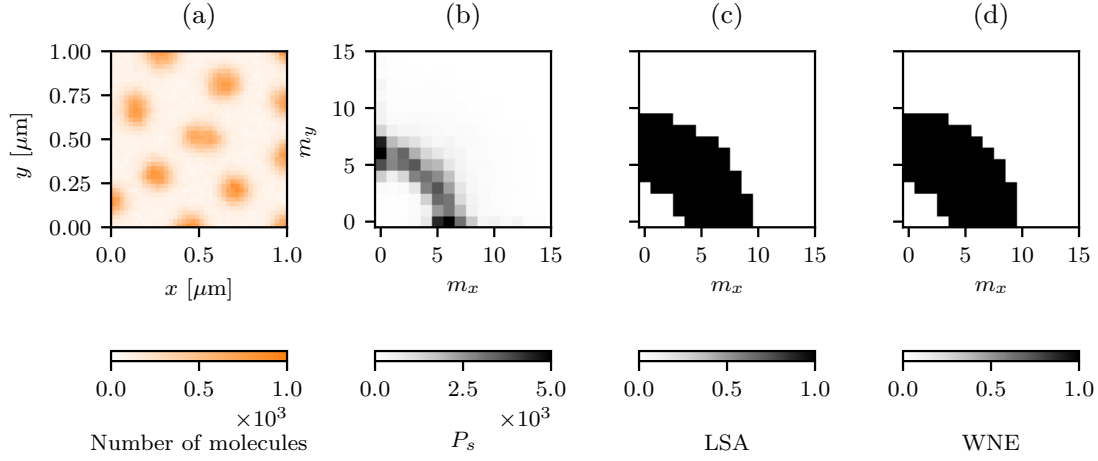


Figure 8: Results from simulations with FVM-derived diffusive jump rates with  $\kappa = 1.0$ . (a) An example pattern of species U. (b) Averaged power spectrum over 100 simulations. (c) Wavemodes predicted using LSA. (d) Wavemodes predicted using the WNE.

385 *The finite element method.* The left-most plot in Figure 9 shows an example pattern  
 386 formed with FEM-derived diffusive jump rates, while the second-from-left plot shows the  
 387 corresponding power spectra averaged over 100 simulations. There is good agreement  
 388 with the possible wavemodes predicted using the WNE (right-most plot of Figure 9) and  
 389 LSA (second-from-right plot of Figure 9).

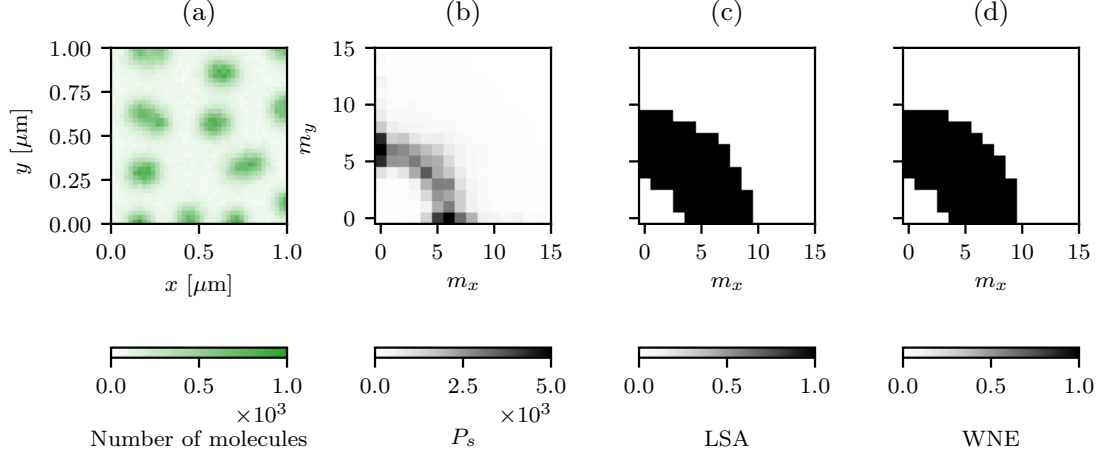


Figure 9: Results from simulations with FEM-derived diffusive jump rates with  $\kappa = 1.0$ . (a) An example pattern of species U. (b) Averaged power spectrum over 100 simulations. (c) Wavemodes predicted using LSA. (d) Wavemodes predicted using the WNE.

390 *The first exit time method.* Lastly, we investigate the effects of using FET-derived diffu-  
 391 sive jump rates on pattern formation. Based on the averaged power spectrum shown in  
 392 Figure 10(b), we see that changing the value of  $\beta$  shifts the range of excited wavemodes  
 393 towards larger values. This observation is consistent with the predictions made using the  
 394 WNE (Figure 10(d)). In this respect, the predictions of LSA fall down as they do not  
 395 take into account details of the diffusive jump rates (Figure 10(c)).

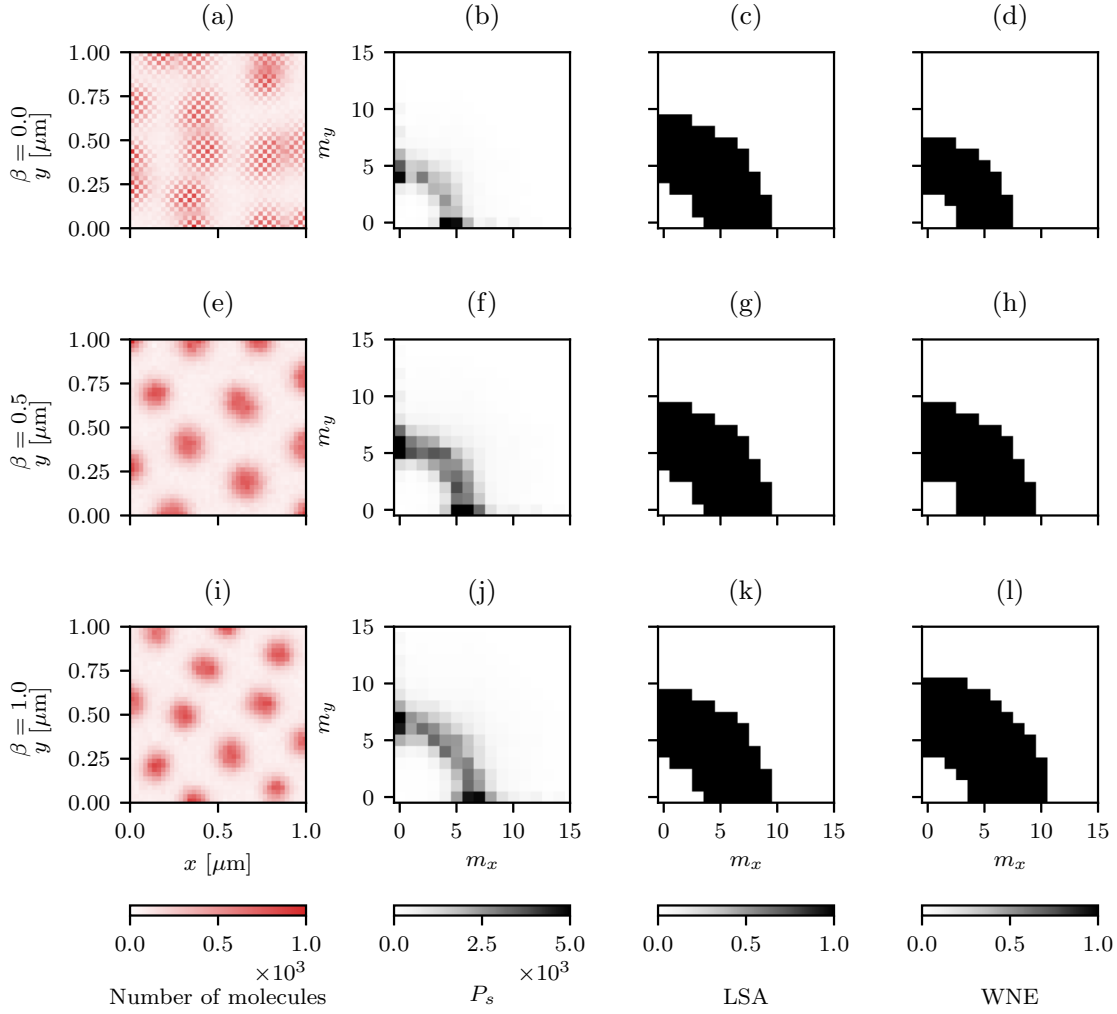


Figure 10: Results from simulations with FET-derived diffusive jump rates with  $\kappa = 1.0$ . (a), (e), (i) An example pattern of species U. (b), (f), (j) Averaged power spectrum over 100 simulations. (c), (g), (k) Wavemodes predicted using LSA. (d), (h), (l) Wavemodes predicted using the WNE. The chequerboard pattern seen in (a) is due to the jump rates being non-zero only in the diagonal directions when  $\beta = 0$ .

396 To explore whether changing the compartment aspect ratio has any bearing on the  
 397 patterns formed, we also simulated the system with  $\kappa = 1.4$ . As in the case of  $\kappa = 1.0$ ,  
 398 larger wavemodes appear as the value of  $\beta$  increases (Figure 11(b)). However, the range  
 399 of wavemodes observed in the  $x$ -direction is more significantly affected than the range in  
 400 the  $y$ -direction. This observation is, again, consistent with the predictions made using  
 401 the WNE, but cannot be predicted using LSA.

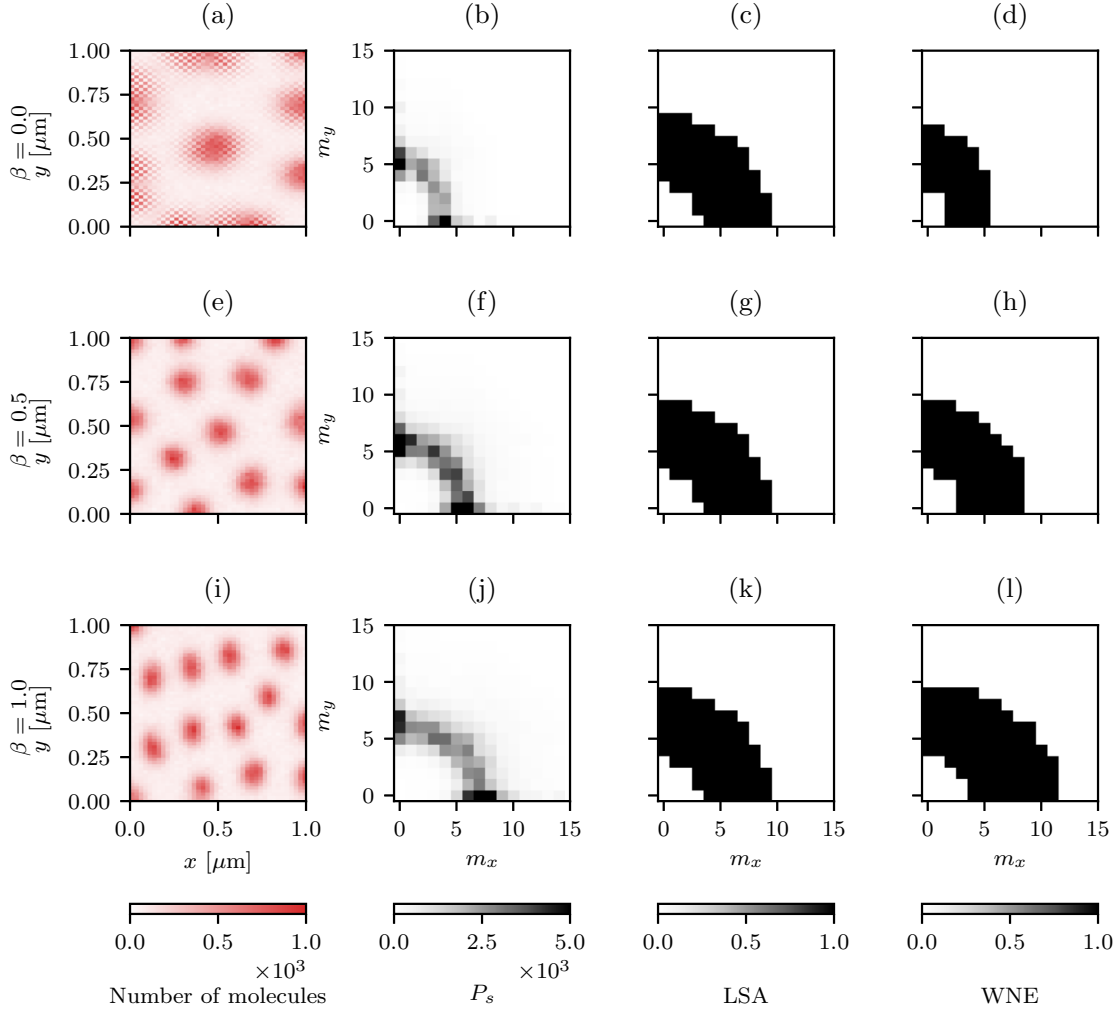
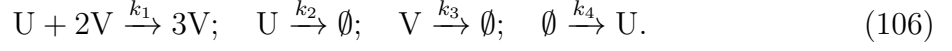


Figure 11: Results from simulations with FET-derived diffusive jump rates with  $\kappa = 1.4$ . (a), (e), (i) An example pattern of species U. (b), (f), (j) Averaged power spectrum over 100 simulations. (c), (g), (k) Wavemodes predicted using LSA. (d), (h), (l) Wavemodes predicted using the WNE. Again, we see checkerboard patterns for  $\beta = 0$  where there are only diagonal jumps.

402 In both cases,  $\kappa = 1.0$  and  $\kappa = 1.4$ , changing the parameter  $\beta$ , which controls the  
 403 rate of molecules jumping diagonally in the FET derivation, has a significant effect on  
 404 the type of patterns formed, as shown in Figure 10 and Figure 11.

### 3.1.5. Gray-Scott kinetics

Another second example of reaction-diffusion kinetics that can exhibit pattern formation via a Turing instability is the Gray-Scott system. Again, the system is composed of two species, U and V, which undergo diffusion (with rates  $D_u$  and  $D_v$ , respectively) and the following reactions:



The corresponding propensity functions are as follows:

$$a_i^1(\mathbf{u}(t), \mathbf{v}(t)) = \frac{k_1}{A(t)^2} u_i(t) v_i(t) (v_i(t) - 1); \quad (107)$$

$$a_i^2(\mathbf{u}(t), \mathbf{v}(t)) = k_2 u_i(t); \quad (108)$$

$$a_i^3(\mathbf{u}(t), \mathbf{v}(t)) = k_3 v_i(t); \quad (109)$$

$$a_i^4(\mathbf{u}(t), \mathbf{v}(t)) = k_4 A(t). \quad (110)$$

All the simulations are run until  $T = 5000 \text{ s}$  on the domain  $\Omega = [0, L] \times [0, L] \mu m^{-2}$ , which is discretised into  $50 \times 50$  compartments. We use the following reaction rates:  $D_u = 0.14 \mu m^2 s^{-1}$ ,  $D_v = 0.06 \mu m^2 s^{-1}$ ,  $k_1 = 2 \times 10^{-5} s^{-1}$ ,  $k_2 = 7.0 s^{-1}$ ,  $k_3 = 0.035 s^{-1}$  and  $k_4 = 0.1 s^{-1}$ . We initialise the system with the following initial condition:

$$u(\mathbf{x}, 0) = \begin{cases} 100 & \text{for } \mathbf{x} \in \left[\frac{3L}{10}, \frac{7L}{10}\right]^2, \\ 200 & \text{otherwise,} \end{cases} \quad (111)$$

$$v(\mathbf{x}, 0) = \begin{cases} 50 & \text{for } \mathbf{x} \in \left[\frac{3L}{10}, \frac{7L}{10}\right]^2, \\ 0 & \text{otherwise.} \end{cases} \quad (112)$$

In Figure 12, we see that, while the method of derivation of the jump rates does not make much of a difference for simulations when the domain is  $\Omega = [0, 50] \times [0, 50] \mu m^{-2}$ , the differences between the methods of derivation in simulations are very pronounced when the domain is  $\Omega = [0, 100] \times [0, 100] \mu m^{-2}$ . In contrast to the Schnakenberg system, the simulations with FEM- and FVM-derived jump rates look very different for the case  $L = 100 \mu m$  and there are far fewer spots when FEM-derived jump rates are used (Figure 12(g)). For simulations with FDM-derived jump rates, as previously, we get a chequerboard pattern when  $L = 50 \mu m$ , however there are no patterns to be found when  $L = 100 \mu m$ . Lastly, simulations with FET-derived jump rates show similar behaviour to

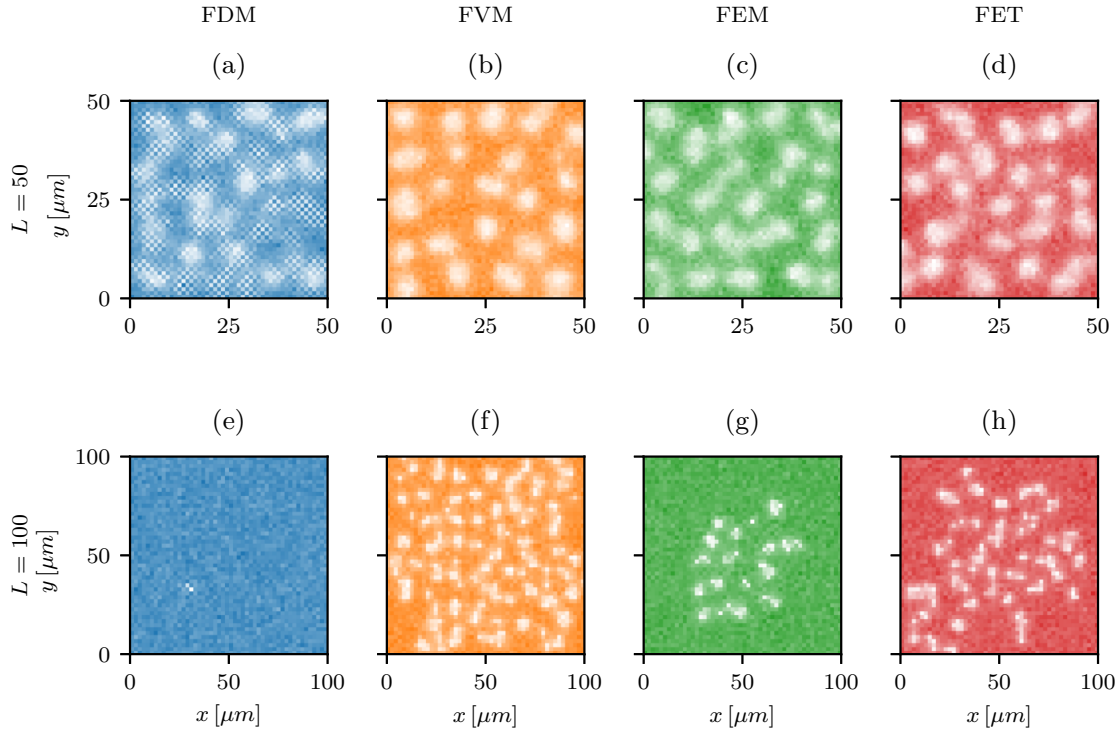


Figure 12: Results from simulations of the Gray-Scott system, showing example patterns of species U at  $T = 5000$  s. (a), (e) show simulations that used FDM-derived jump rates with  $\alpha = 1.0$ . (b), (f) show simulations that used FVM-derived jump rates. (c), (g) show the simulations that used FEM-derived jump rates. (d), (h) show the simulations that used the FET-derived jump rates with  $\beta = 0.5$ . The row that contains (a), (b), (c), (d) shows simulations where the domain is  $\Omega = [0, 50] \times [0, 50] \mu m^{-2}$ , *i.e.*  $L = 50 \mu m$ , while the row that contains (e), (f), (g), (h) shows simulations where the domain is  $\Omega = [0, 100] \times [0, 100] \mu m^{-2}$ , *i.e.*  $L = 100 \mu m$ .

simulations with FEM-derived jump rates, in that when  $L = 50 \mu m$  spots appear over the whole domain, while when  $L = 100 \mu m$  spots appear in a subset of the domain.

The results in this section highlight just how much of a difference the use of different derivations of the jump rates can have on simulation results, and hence model predictions.



### 3.2. Growing domain

In this section, we explore the effects of using the different diffusive jump rate derivations on a growing domain. As for the static domain case, we first consider cases where we can compare with the analytic solution of the corresponding macroscale PDE and we then consider models for pattern formation. We assume domain growth to be isotropic, such that  $\Omega_t = [0, L(t)]^2 \mu m^{-2}$  and, for simplicity, we consider the domain to be growing exponentially in time so that

$$L(t) = L_0 e^{rt}, \tag{113}$$

where  $L_0$  is the initial domain size and  $r$  the growth rate.

As we now have time-dependent propensity functions, we cannot use the simulation algorithm as stated in Section 2. We adapt Algorithm 1 using the Extrande method [30]. As each of the propensity functions decreases with time, we use the propensity function calculated at time  $t$  as the upper bound in the time interval,  $[t, t + \delta t]$  in the Extrande method. Hence, the modified SSA we use is as stated in Algorithm 2.

---

**Algorithm 2** Modified next sub-volume method SSA

---

Set  $t = 0$ .

Initialise  $\mathbf{u}$ .

**for**  $i$  in  $\{1, 2, \dots, I\}$  **do**

    Calculate the total propensity in compartment  $i$ ,  $a_i^0(\mathbf{u}(t), t)$ .

    Set the upper bound  $\tilde{a}_i(\mathbf{u}(t), t) = a_i^0(\mathbf{u}(t), t)$

    Initialise the time until the next reaction for compartment  $i$ :  $t_i \sim \exp(\tilde{a}_i(\mathbf{u}(t), t))$ .

**end for**

**while**  $t < T$  **do**

    Find argmin of the set  $\{t_1, t_2, \dots, t_I\}$  and denote it  $m$ .

    Set  $t = t_m$ .

    Generate a random number  $r \sim U(0, 1)$ .

    Choose reaction / diffusion  $q$  to fire. Note that reaction  $k$  fires with probability  $a_i^k(\mathbf{u}(t), t) / \tilde{a}_i(\mathbf{u}(t), t)$ , diffusion of a molecule of species  $\varsigma$  from box  $i$  to box  $j$  occurs with probability  $d_{i,j}^\varsigma(\mathbf{u}(t), t) / \tilde{a}_i(\mathbf{u}(t), t)$  and no reaction happens with probability  $(\tilde{a}_i(\mathbf{u}(t), t) - a_i^0(\mathbf{u}(t), t)) / \tilde{a}_i(\mathbf{u}(t), t)$ .

    Update molecule numbers:  $\mathbf{u} := \mathbf{u} + \boldsymbol{\nu}_q$ , where  $\boldsymbol{\nu}_q$  is the stoichiometric matrix of reaction / diffusion  $q$ .

    Let  $\Gamma$  be the set of indices of non-zero elements of  $\boldsymbol{\nu}_q$ .

**for**  $\gamma$  in  $\Gamma$  **do**

        Update  $a_\gamma^k(\mathbf{u}(t), t)$ ,  $d_{\gamma,j}^\varsigma(\mathbf{u}(t), t)$ ,  $a_\gamma^0(\mathbf{u}(t), t)$  and  $\tilde{a}_\gamma(\mathbf{u}(t), t)$  accordingly.

        Generate a random number  $\Delta t \sim \exp(\tilde{a}_\gamma(\mathbf{u}(t), t))$ .

        Update the time until the next reaction:  $t_\gamma = t + \Delta t$ .

**end for**

**end while**

---

As in the static case, there is an analytic solution to the macroscale PDE and it is given by (for derivation of this result we direct the reader to [25])

$$\begin{aligned}
u(\mathbf{x}, t) = & \frac{u_0 \kappa h^2}{L_0^2} \exp(-2rt) \\
& + \sum_{n=1}^{\infty} \frac{2u_0 h}{n\pi L_0} \sin\left(\frac{n\pi \kappa h}{L_0}\right) \cos\left(\frac{n\pi x}{L_0}\right) \exp\left(-\frac{D}{2r} \left(\frac{n\pi}{L_0}\right)^2 (1 - \exp(-2rt)) - 2rt\right) \\
& + \sum_{m=1}^{\infty} \frac{2u_0 \kappa h}{m\pi L_0} \sin\left(\frac{m\pi h}{L_0}\right) \cos\left(\frac{m\pi y}{L_0}\right) \left(-\frac{D}{2r} \left(\frac{m\pi}{L_0}\right)^2 (1 - \exp(-2rt)) - 2rt\right) \\
& + \sum_{n=1}^{\infty} \sum_{m=1}^{\infty} \frac{4u_0}{nm\pi^2 L_0^2} \sin\left(\frac{n\pi \kappa h}{L_0}\right) \sin\left(\frac{m\pi h}{L_0}\right) \cos\left(\frac{m\pi x}{L_0}\right) \cos\left(\frac{n\pi y}{L_0}\right) \\
& \times \exp\left(-\frac{D}{2r} \frac{(n^2 + m^2)\pi^2}{L_0^2} (1 - \exp(-2rt)) - 2rt\right).
\end{aligned} \tag{114}$$

Figure 13 shows how the error between the results of stochastic simulation and the analytic solution, as defined in Section 3.1, evolves in time. We can see that in all the cases shown in Figure 13, whether for a static or a growing case, the error decreases with time and that the simulations with FVM-derived diffusive jump rates have the lowest error.

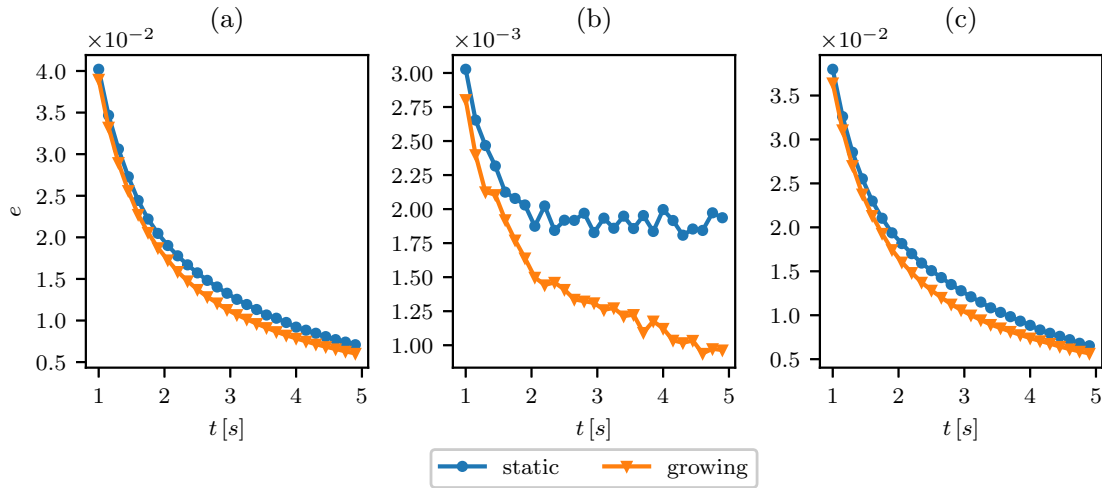


Figure 13: Plots of the error,  $e(t)$ , as a function of time for simulations with diffusion coefficient  $D = 1 \mu\text{m}^2\text{s}^{-1}$  and growth rate  $r = 0.1\text{s}^{-1}$ . In each plot we compare the errors from simulations for a static domain and a growing domain where the jump rates were derived using: (a) the FDM ( $\alpha = 0.9$ ); (b) the FVM; and (c) the FEM. The domain, of initial size  $[0, 5] \times [0, 5] \mu\text{m}^{-2}$ , has been discretised into  $21 \times 21$  compartments and all  $5 \times 10^6$  molecules are initially placed into the bottom-right compartment.

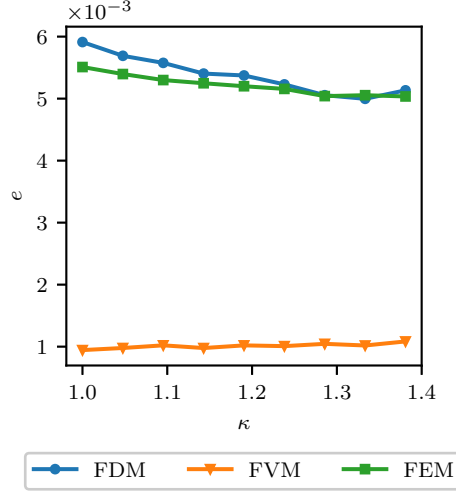


Figure 14: Plots of the error,  $e(t)$ , as a function of voxel aspect ratio,  $\kappa$ , at time  $t = 5.0$  s for simulations with diffusion coefficient  $D = 1 \mu m^2 s^{-1}$  and growth rate  $r = 0.1 s^{-1}$ . We compare different derivations of the diffusive jump rates as we vary  $\kappa$ . For the FDM,  $\alpha = 0.7$ . The domain, of initial size  $[0, 5] \times [0, 5] \mu m^{-2}$ , is discretised into  $21 \times 21\kappa$  compartments and all  $5 \times 10^6$  molecules are initially placed into the bottom-right compartment.

Next, we explore the effects of changing the voxel aspect ratio,  $\kappa$ , on the error, presenting results in Figure 14. The FVM-derived diffusive jump rates provide the smallest error across the range of compartment aspect ratios considered, increasing slightly as the aspect ratio increases. On the other hand, for both the FEM- and FVM-derived diffusive jump rates, there is a slight decrease in the error as the compartment aspect ratio is increased.

### 3.2.2. Schnakenberg kinetics

We now consider pattern formation on a growing domain to determine to what extent the different derivations of diffusive jump rates affect the patterns formed. We first use the Schnakenberg system, as in Section 3.1.4. Figure 15 showcases the range of patterns that form as the domain growth rate is varied.

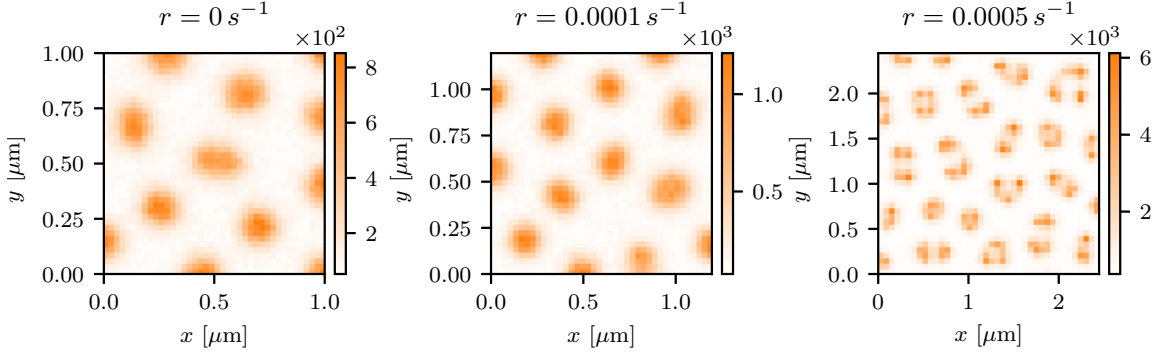


Figure 15: Comparison of different growth rates for simulations of the Schnakenberg system with the following parameters:  $D_u = 1 \times 10^{-5} \mu m^2 s^{-1}$ ,  $D_v = 0.001 \mu m^2 s^{-1}$ ,  $k_1 = 1.0 \mu m^{-2} s^{-1}$ ,  $k_2 = 0.02 s^{-1}$ ,  $k_3 = 1 \times 10^{-6} \mu m^4 s^{-1}$ ,  $k_4 = 3.0 \mu m^{-2} s^{-1}$  run until  $T = 1800 s$  and FVM-derived jump rates are used. The domain, of initial size  $[0, 1] \times [0, 1] \mu m^{-2}$ , is discretised into  $40 \times 40$  compartments.

We see in Figure 16 that the patterns formed are different compared to the static case. However, using different derivations for the diffusive jump rates does not seem to markedly affect the patterns produced. The reason we see different patterns when the domain grows is because higher wavemodes become available, and the inherent stochasticity in the system causes clusters of molecules (peaks) to split and these higher wavemodes are then realised. This change in the wavemode is highlighted in the centre and left-hand columns in Figure 16.

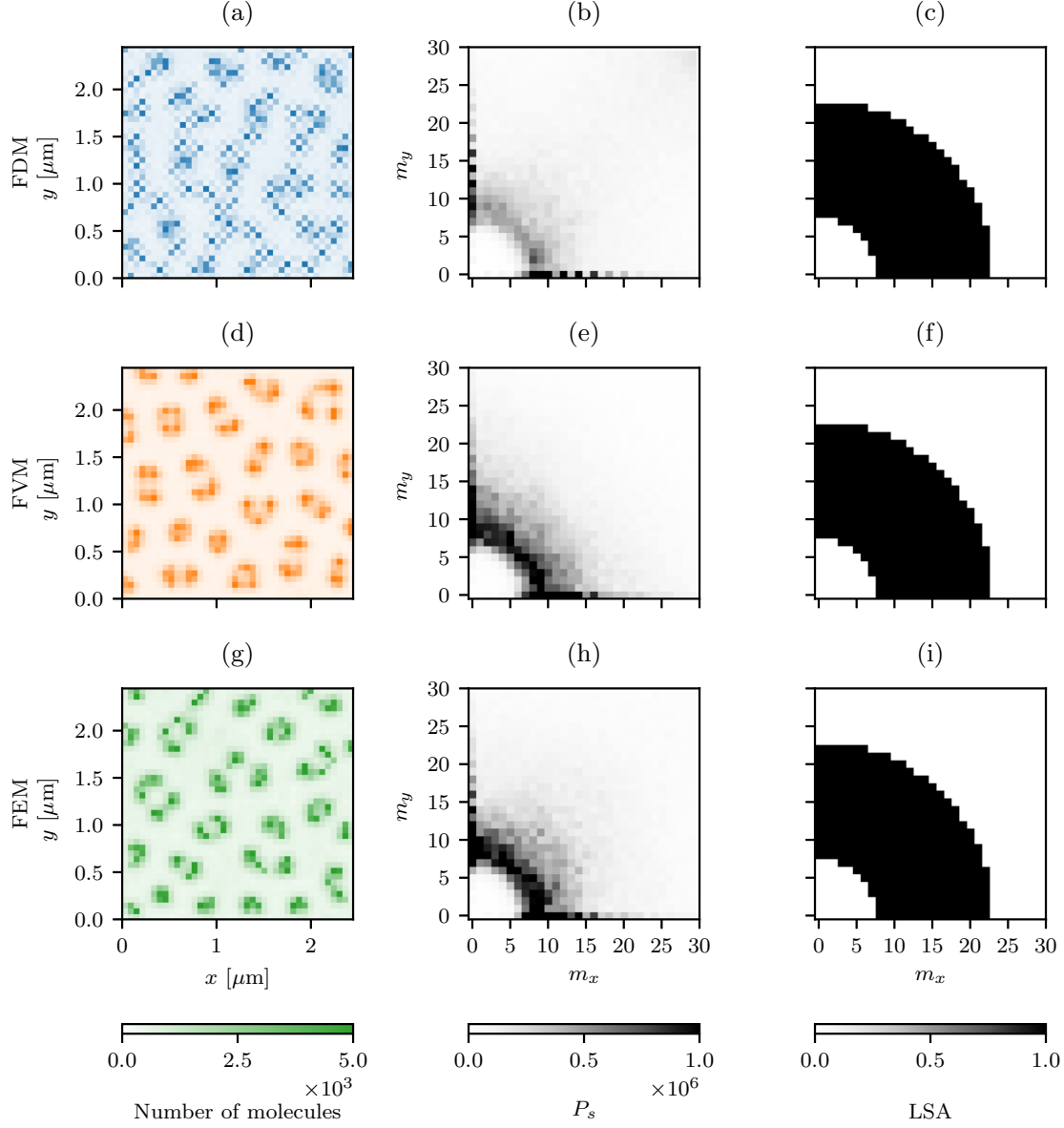


Figure 16: Results from simulations of the Schnakenberg system on a growing domain with the following parameters:  $D_u = 1.0 \times 10^{-5} \mu m^2 s^{-1}$ ,  $D_v = 0.001 \mu m^2 s^{-1}$ ,  $k_1 = 1.0 \mu m^{-2} s^{-1}$ ,  $k_2 = 0.02 s^{-1}$ ,  $k_3 = 1 \times 10^{-6} \mu m^4 s^{-1}$ ,  $k_4 = 3.0 \mu m^{-2} s^{-1}$  run until  $T = 1800 s$ . In the top row, for the FDM results, a value of  $\alpha = 1.0$  was used. The domain, of initial size  $[0, 1] \times [0, 1] \mu m^{-2}$ , is discretised into  $40 \times 40$  compartments. Left-hand column – example patterns; centre column – averaged power spectrum over 100 simulations; right-hand column – predictions from LSA.

### 3.2.3. *Gray-Scott kinetics*

Finally, we consider the Gray-Scott system, as in Section 3.1.5. In Figure 17 we see that on a growing domain, unlike in the Schnakenberg case, the choice of discretisation method has a strong effect on pattern formation. We see that when the domain is growing exponentially, spots form by the end of simulations irrespective of the method of jump rate derivation (Figure 17(d), (e) and (f)). In the cases where the domain grows exponentially in Figure 17, the domain size is  $[0, 50]^2 \mu m^{-2}$  initially and grows to be  $[0, 100]^2 \mu m^{-2}$  by the end of the simulations. For comparison we also show results from simulations where the domain is static and of sizes  $[0, 50]^2 \mu m^{-2}$  and  $[0, 100]^2 \mu m^{-2}$ . We see that even though the patterns do not completely form when FDM- and FEM-derived jump rates are used on the domain  $[0, 100]^2 \mu m^{-2}$ , patterns do form in the case of an exponentially growing domain.

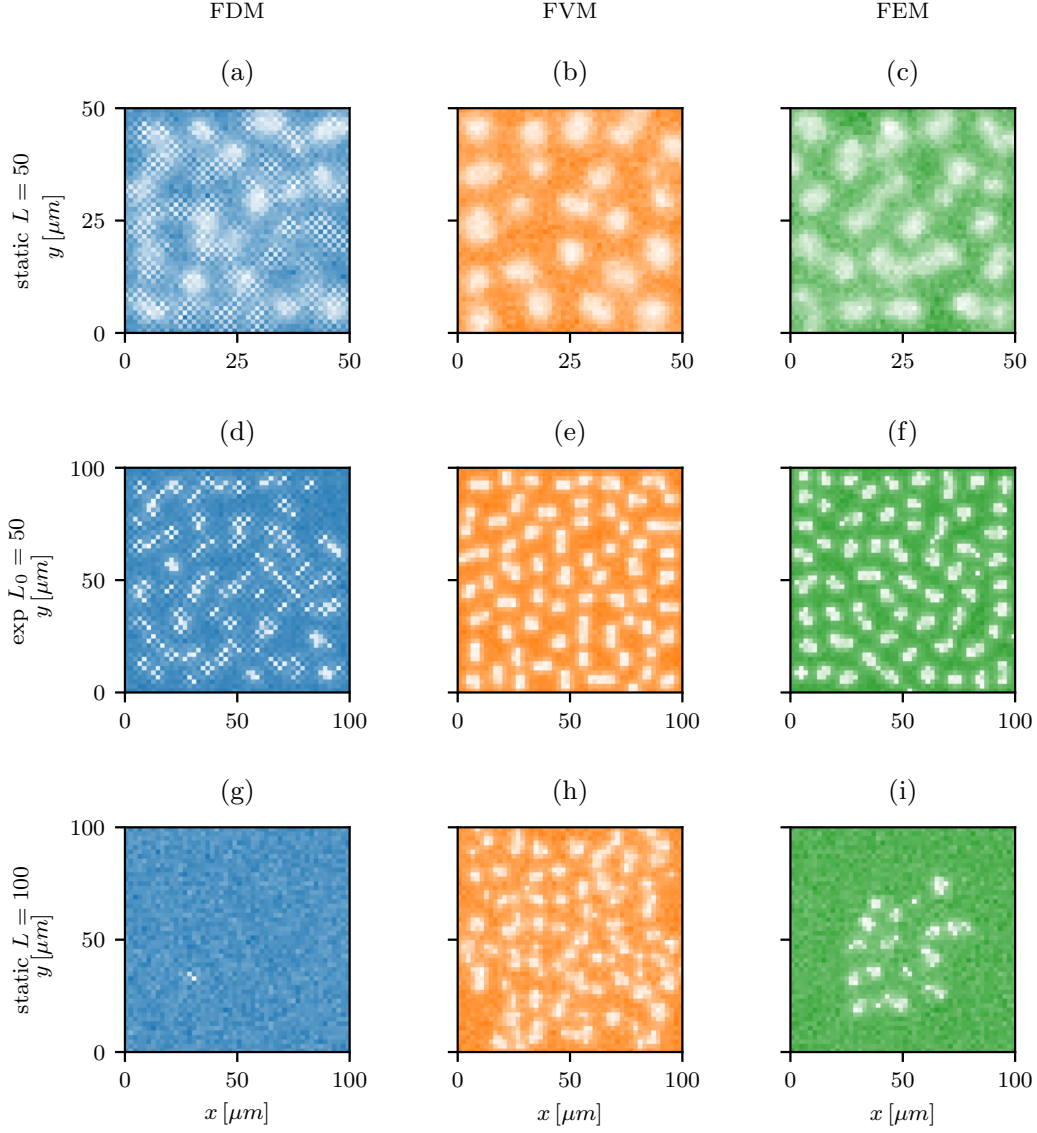


Figure 17: Results from simulations of the Gray-Scott system, at  $T = 5000$  s. (a), (d), (g) show simulations that used FDM-derived jump rates with  $\alpha = 1.0$ . (b), (e), (h) show simulations that used FVM-derived jump rates. (c), (f), (i) show the simulations that used FEM-derived jump rates. The row that contains (a), (b), (c) shows simulations where the domain is  $\Omega = [0, 50] \times [0, 50] \mu m^{-2}$ , *i.e.*  $L = 50 \mu m$ . The row that contains (d), (e), (f) shows simulations where the domain is growing at an exponential rate, *i.e.*  $L = L_0 e^{rt}$ , where  $L_0 = 50 \mu m$  and  $r = 1.39 \times 10^{-4} s^{-1}$ , such that at the end of the simulation the domain is  $L(5000) = 100 \mu m$ . The last row shows the results of simulations on the static domain  $\Omega = [0, 100] \times [0, 100] \mu m^{-2}$ .



## 4. Conclusions

Our aim in this work was to investigate the effects of different methods of derivation of diffusive jump rates on stochastic reaction-diffusion systems modelled using the RDME. To do so, we replicated, extended and applied the results of Meinecke and Lötstedt [18] to a number of reaction-diffusion systems, that included a range of reaction types, on both static and growing domains.

For the production-decay examples, which consisted solely of zeroth and first order reactions, the FVM generally gives the most reliable results in terms of the error between stochastic simulations and solution of the corresponding macroscale PDE (as does the FDM for  $\alpha = 0$  where there are no diagonal jumps and we have the same diffusive jump rates as for the FVM) (Figure 5). When bimolecular reactions are included, we showed that the spatial discretisation affects results, for example shifting the stationary distribution (Figure 6).

We then moved to study the effects of different methods of derivation of diffusive jump rates on pattern formation, using the Turing reaction-diffusion model with both Schnakenberg and Gray-Scott kinetics as examples. We compared the averaged power spectra from simulations with the wavemodes predicted using LSA, which analyses the corresponding PDE model, and the WNE, which takes into account the details of the diffusive jump rates (Figures 7–10). Our results show that the WNE approach provides good predictions of the range of possible wavemodes, as expected from the work of Woolley *et al.* [32]. In particular, we showed that the aspect ratio of the compartments can significantly affect the patterns formed (see Figure 11).

We also considered the effects of uniform domain growth on derivations of the diffusive jump rates, and simulations of pattern formation. We considered the FDM, FVM and FEM showing, in line with the results of Woolley *et al.* [32], that the diffusive jump rates become time-dependent as the compartment dimensions now change over time. It is not possible to use the FET approach in the context of growing domains because the mean of the FET distribution becomes infinite, and it is difficult to approximate the FET distribution with an exponential distribution. For the Gray-Scott system we saw the choice of method of derivation of the jump rates can significantly impact the patterns formed.

Taken together, the results presented in this work demonstrate that care should be

taken when choosing how to model diffusion in the context of RDME models of stochastic reaction-diffusion systems. Future work will consider how to extend these results to unstructured meshes and more complicated forms of domain growth, such as non-uniform growth of the domain. Furthermore, derivations of theoretical estimates of the errors, that show the dependence on the method of derivation and any algorithm parameters, are left as future work.

## Acknowledgements

R.E.B. is a Royal Society Wolfson Research Merit Award holder, would like to thank the Leverhulme Trust for a Research Fellowship. B.J.B. would like to thank the EPSRC for supporting this research through grant EP/G03706X/1.

## References

- [1] S. S. Andrews and D. Bray. Stochastic simulation of chemical reactions with spatial resolution and single molecule detail. *Physical Biology*, 1(3):137, 2004.
- [2] J. Elf and M. Ehrenberg. Spontaneous separation of bi-stable biochemical systems into spatial domains of opposite phases. *Systems Biology*, 1(2):230–236, 2004.
- [3] H. C. Elman, D. J. Silvester, and A. J. Wathen. *Finite Elements and Fast Iterative Solvers: With Applications in Incompressible Fluid Dynamics*. Oxford University Press, 2010.
- [4] M. B. Elowitz, A. J. Levine, E. D. Siggia, et al. Stochastic gene expression in a single cell. *Science*, 297(5584):1183–1186, 2002.
- [5] S. Engblom, L. Ferm, A. Hellander, and P. Lötstedt. Simulation of stochastic reaction-diffusion processes on unstructured meshes. *SIAM Journal on Scientific Computing*, 30(6):2709–2733, 2008.
- [6] R. Erban, S. J. Chapman, and P. K. Maini. A practical guide to stochastic simulations of reaction-diffusion processes. arXiv preprint, 2007.
- [7] A. Gierer and H. Meinhardt. A theory of biological pattern formation. *Kybernetik*, 12(1):30–39, 1972.

- [8] D. T. Gillespie. A general method for numerically simulating the stochastic time evolution of coupled chemical reactions. *Journal of Computational Physics*, 22(4):403–434, 1976.
- [9] J. Hattne, D. Fange, and J. Elf. Stochastic reaction-diffusion simulation with MesoRD. *Bioinformatics*, 21(12):2923–2924, 2005.
- [10] S. Hellander and L. Petzold. Reaction rates for reaction-diffusion kinetics on unstructured meshes. *Journal of Chemical Physics*, 146(6), 2017.
- [11] M. Howard and A. D. Rutenberg. Pattern formation inside bacteria: fluctuations due to the low copy number of proteins. *Physical Review Letters*, 90(12):128102, 2003.
- [12] S. A. Isaacson. The reaction-diffusion master equation as an asymptotic approximation of diffusion to a small target. *SIAM Journal on Applied Mathematics*, 70(1):77–111, 01 2009.
- [13] S. A. Isaacson. A convergent reaction-diffusion master equation. *Journal of Chemical Physics*, 139(5), 2013.
- [14] S. A. Isaacson, D. M. McQueen, and C. S. Peskin. The influence of volume exclusion by chromatin on the time required to find specific DNA binding sites by diffusion. *Proceedings of the National Academy of Sciences*, 2011.
- [15] D. Longo and J. Hasty. Dynamics of single-cell gene expression. *Molecular Systems Biology*, 2(1):64, 2006.
- [16] P. Lötstedt and L. Meinecke. Simulation of stochastic diffusion via first exit times. *Journal of Computational Physics*, 300:862–886, 2015.
- [17] L. Meinecke, S. Engblom, A. Hellander, and P. Lötstedt. Analysis and design of jump coefficients in discrete stochastic diffusion models. *SIAM Journal on Scientific Computing*, 38(1):A55–A83, 2016.
- [18] L. Meinecke and P. Lötstedt. Stochastic diffusion processes on Cartesian meshes. *Journal of Computational and Applied Mathematics*, 294:1–11, 2016.
- [19] R. L. Mort, R. J. H. Ross, K. J. Hainey, O. J. Harrison, M. A. Keighren, G. Landini, R. E. Baker, K. J. Painter, I. J. Jackson, and C. A. Yates. Reconciling diverse

mammalian pigmentation patterns with a fundamental mathematical model. *Nature Communications*, 7(1):10288, 2016.

[20] J. D. Murray. *Mathematical Biology II: Spatial Models and Biomedical Applications*. Springer-Verlag New York Incorporated, 2001.

[21] J. M. Osborne, A. G. Fletcher, J. M. Pitt-Francis, P. K. Maini, and D. J. Gavaghan. Comparing individual-based approaches to modelling the self-organization of multicellular tissues. *PLoS Computational Biology*, 13(2):1–34, 2017.

[22] S. Redner and J. R. Dorfman. A guide to first-passage processes. *American Journal of Physics*, 70(11):1166–1166, 2002.

[23] J. Schnakenberg. Simple chemical reaction systems with limit cycle behaviour. *Journal of Theoretical Biology*, 81(3):389–400, 1979.

[24] D. Schnoerr, G. Sanguinetti, and R. Grima. Approximation and inference methods for stochastic biochemical kinetics—a tutorial review. *Journal of Physics A: Mathematical and Theoretical*, 50(9):093001, 2017.

[25] M. J. Simpson and R. E. Baker. Exact calculations of survival probability for diffusion on growing lines, disks, and spheres: The role of dimension. *Journal of Chemical Physics*, 143(9):94109, 2015.

[26] J. C. Strikwerda. *Finite Difference Schemes and Partial Differential Equations*, volume 88. SIAM, 2004.

[27] A. M. Turing. The chemical basis of morphogenesis. *Philosophical transactions of the Royal Society of London. Series B, Biological sciences*, 237(641):37–72, 1952.

[28] N. G. van Kampen. *Stochastic Processes in Physics and Chemistry*. North Holland Personal Library. Elsevier, Oxford, 3rd edition, 2007.

[29] P. Van Liedekerke, M. M. Palm, N. Jagiella, and D. Drasdo. Simulating tissue mechanics with agent-based models: concepts, perspectives and some novel results. *Computational Particle Mechanics*, 2(4):401–444, 2015.

- [30] M. Voliotis, P. Thomas, R. Grima, and C. G. Bowsher. Stochastic simulation of biomolecular networks in dynamic environments. *PLoS Computational Biology*, 12(6):e1004923, 2016.
- [31] A. Volkening and B. Sandstede. Modelling stripe formation in zebrafish: an agent-based approach. *Journal of The Royal Society Interface*, 12(112):20150812, 2015.
- [32] T. E. Woolley, R. E. Baker, E. A. Gaffney, and P. K. Maini. Power spectra methods for a stochastic description of diffusion on deterministically growing domains. *Physical Review E*, 84(2), 2011.
- [33] T. E. Woolley, R. E. Baker, E. A. Gaffney, and P. K. Maini. Stochastic reaction and diffusion on growing domains: understanding the breakdown of robust pattern formation. *Physical Review E*, 84(4):46216, 2011.